The inner scaffold protects from centriole fracture

Emmanuelle Steib[1], Davide Gambarotto[1†], Marine H. Laporte[1†], Natacha Olieric[2], Céline Zheng[2*], Susanne Borgers[1], Vincent Olieric[3], Maeva Le Guennec[1], France Koll[4], Anne-Marie Tassin[4], Michel O. Steinmetz[2,5], Virginie Hamel[1§] and Paul Guichard[1§]

[1] University of Geneva, Department of Cell Biology, Sciences III, Geneva, Switzerland

[2] Laboratory of Biomolecular Research, Division of Biology and Chemistry, Paul Scherrer Institut, Villigen, Switzerland

[3] Swiss Light Source, Paul Scherrer Institut, 5232 Villigen, Switzerland

[4] Institute for Integrative Biology of the Cell (I2BC), CEA, CNRS, Univ. Paris Sud, Université Paris-Saclay, 1 Avenue de la Terrasse, 91198 Gif sur Yvette, France.

[5] Biozentrum, University of Basel, 4056 Basel, Switzerland

* Present address: Department of Biochemistry, University of Oxford, South Parks Road, Oxford, OX1 3QU, UK

† These authors contributed equally to this work.

§ Correspondence to: virginie.hamel@unige.ch and paul.guichard@unige.ch

Abstract:

Centrioles are characterized by a nine-fold arrangement of microtubule triplets held together by an inner protein scaffold. While performing their functions, these organelles experience strenuous cellular forces without breaking. What maintains centriole integrity is a fundamental question that remains poorly understood. Here, we reveal the function of the inner scaffold in imparting centriole cohesion by studying POC16 and its human homolog WDR90. We unveil POC16/WDR90, as microtubule-binding proteins that localize on the microtubule wall along the central core region of the centriole and interact with the inner scaffold components FAM161A and POC5. Strikingly, WDR90/POC16 depletion impairs the inner scaffold, leading to structural abnormalities and centriole fracture in human and *Chlamydomonas* cells. This work highlights the importance of the inner scaffold in protecting centriole architecture.

One Sentence Summary:

Centriole integrity is ensured by the connection between the inner scaffold and microtubule triplets through POC16/WDR90 proteins.

Main Text:

Centrioles and basal bodies (referred to as centrioles from here onwards for simplicity) are conserved organelles important for the formation of the centrosome, the major microtubule-organizing center of animal cells, as well as for templating cilia and flagella (*1–4*). Consequently, defects in centriole assembly, size, structure and number lead to abnormal mitosis or defective ciliogenesis and have been associated with several human pathologies such as

ciliopathies and cancer (*5*–*7*). For instance, centriole amplification, a hallmark of cancer cells, can result from centriole fragmentation in defective, over-elongated centrioles (*8*).

Centrioles are characterized by a nine-fold radial arrangement of microtubule triplets, are polarized along their long axis, and can be divided in three distinct regions termed proximal end, central core and distal tip (*9*). Each region displays peculiar structural features such as the cartwheel on the proximal end, which is crucial for centriole assembly (*10*, *11*) or the distal appendages at the very distal region, essential for membrane docking during ciliogenesis (*12*). The central core region of the centriole is defined by the presence of a circular inner scaffold that maintains the cohesion of microtubule triplets under compressive forces (Le Guennec et al, in press). Using cryo-tomography, we recently showed that the inner centriole scaffold forms an extended helix covering ~70% of the centriole length and that is rooted at the inner junction between the A and B microtubules (Fig. 1A, B). This connection consists of a stem attaching the neighboring A and B microtubules and three arms extending from the same stem toward the centriolar lumen (Le Guennec et al, in press) (Fig. 1A, B). The stem of the inner scaffold has been detected in *Paramecium tetraurelia*, *Chlamydomonas reinhardtii* and human centrioles, suggesting that it represents an evolutionary conserved structural feature.

The molecular identity of some components of the inner scaffold has been uncovered using Ultrastructure Expansion Microscopy (U-ExM), which allows nanometric localization of proteins within structural elements (*13*). Notably, the centriolar proteins POC1B, FAM161A, POC5 and Centrin-2 have been shown to localize to the inner scaffold along the microtubule blades in human cells (Le Guennec et al, in press). Moreover, these proteins form a complex that can bind to microtubules through the microtubule-binding protein FAM161A (*14*) (Le Guennec et al., in press). Importantly, a subset of these proteins has been shown to be important for

centriole elongation (*15*) as well as for centriole and basal body integrity (*16*, *17*). This observation highlights the prominent role of the inner scaffold structure in providing stability to the entire centriolar microtubule wall organization. However, this hypothesis has not been challenged up to now and the exact contribution of the inner scaffold to microtubule triplets cohesion and how the inner scaffold is connected to the microtubule blade is unknown.

We recently identified the conserved proteins POC16/WDR90 as proteins localizing to the central core region in both *Chlamydomonas reinhardtii* and human centrioles (*9*), which is also covered by the inner scaffold structure. Impairing POC16 or WDR90 functions has been found to affect ciliogenesis, suggesting that POC16/WDR90 stabilizes the microtubule wall, thereby ensuring proper flagellum or cilium assembly (Hamel et al, 2017). Interestingly, POC16 has been proposed to be at the inner junction between the A and B microtubules (*18*) through its homology with FAP20, an axonemal microtubule doublet inner junction protein of *Chlamydomonas reinhardtii* flagella (*19–21*). As the stem connects the A- and B-microtubules interface, these observations suggest that POC16/WDR90 may connect the inner scaffold to the microtubule triplet through this stem structure, thus ensuring centriole cohesion (Fig. 1C).

In this study, using a combination of cell biology, biochemistry and Ultrastructure Expansion Microscopy (U-ExM) approaches, we establish that the conserved POC16/WDR90 proteins localize on the centriolar microtubule wall in the central core region of both *Chlamydomonas* and human cells centrioles. We further demonstrate that WDR90 is a microtubule-binding protein that recruits inner scaffold components and that loss of this protein leads to a slight centriole elongation, impairment of the canonical circular shape of centrioles as well as centriolar fracture in both species. Our results highlight that the essential role of POC16/WDR90 is in recruiting the inner scaffold and maintaining the architecture of centrioles.

Results

POC16/WDR90 is a conserved microtubule wall component of the central core region

To test the hypothesis that POC16/WDR90 is a microtubule triplet component, we analyzed its distribution using U-ExM. We observed that the endogenous POC16 longitudinal fluorescence signal is restricted to the central core region as compared to the tubulin signal depicting total centriolar length (Fig. 1D, F, G). From top viewed centrioles, we measured both POC16 and tubulin maximal intensity signals from the exterior to the interior of the centriole and quantified the shift between x-values (Fig. 1E, H, shift between POC16 and tubulin $\Delta = 0$ nm). We concluded that POC16 localizes precisely on the microtubule wall in the central core region of *Chlamydomonas* centrioles. As a control, we could recapitulate the internal localization along the microtubule wall of POB15, another central core protein (Fig. 1I-M) as previously reported using immunogold-labeling (*9*). Furthermore, the POC16 human homolog WDR90 localizes, similarly to POC16, on the centriolar microtubule wall, demonstrating the evolutionary conserved localization of POC16/WDR90 on microtubule triplets in the central core region of centrioles (Fig. 1N-R).

Next, we compared the relative position of WDR90 to previously described inner scaffold components (Fig. 1R-T). We found that while WDR90 precisely localizes to the centriolar microtubule wall (Fig. 1R, x-value for maximal fluorescent signal shift between WDR90 and tubulin: Δ= 2nm), POC1B, FAM161A, POC5 and Centrin-2 signals were shifted towards the centriole lumen in comparison to the tubulin signal, as previously reported (Fig. 1S, Δ= 14 to 30nm) (Le Guennec et al, in press).

POC16/WDR90 is an evolutionary conserved microtubule associated protein that forms a complex with FAM161A and POC5

Proteins of the POC16/WDR90 family consist of an N-terminal DUF667-containing domain (domain of unknown function), homologous to the ciliary inner junction protein FAP20 (Fig. S1A) (Yanagisawa et al., 2014), which is followed by multiple WD40 repeats that form β-propeller structures (Fig. 2A and Fig. S1B) (*22*).

First, we wanted to probe the evolutionary conservation of POC16/WDR90 family members as centriolar proteins. To this end, we raised an antibody against *Paramecium tetraurelia* POC16 and confirmed its localization at centrioles similarly to what we found in *Chlamydomonas reinhardtii* and human cells (Fig. S1C) (Hamel et al., 2017).

Further driven by its predicted homology to FAP20 and the underlying hypothesis that POC16/WDR90 proteins might be joining A and B microtubules as well as by their precise localization on the microtubule wall, we first set out to understand the structural homology between the predicted structures of POC16-DUF667 domain to the recently published near atomic structure of FAP20 from flagella microtubule doublets (*23*) (Fig. S2A-C). Strikingly, we observed high similarities between the two structures, suggesting similar biological functions at the inner junction. Moreover, we fitted POC16 model prediction into FAP20 cryo-EM density map and found a good concordance, further hinting for a conserved localization at the level of the microtubule triplet (Fig. S2D).

Prompted by this result, we then tested whether POC16/WDR90 proteins can bind microtubules both *in vivo* and *in vitro*. To do so, we overexpressed the N-terminal part of WDR90 and crPOC16 comprising the DUF667 domain (WDR90-N(1-225) and CrPOC16(1-295), respectively, fused to GFP in U2OS cells and found that this region is sufficient to decorate

cytoplasmic microtubules *in vivo* (Fig. 2B and S3A). We next tested whether overexpressing such a WDR90-N-terminal fragment could stabilize microtubules. To this end, we analyzed the microtubule network in cells overexpressing mCherry-WDR90-N after depolymerizing microtubules through a cold shock treatment (Fig. S3B-D). We found that while low expressor cells did not maintain a microtubule network, high expressor cells did. This suggests that WDR90-N can stabilize microtubules. In contrast, we observed that full-length WDR90 fused to GFP only anecdotally binds microtubules *in vivo*, possibly due to an autoinhibited conformation of the full-length protein and/or to interacting partners preventing microtubule binding in cells (Fig. S3E, Fig. 2H).

Next, we determined whether different POC16/WDR90 N-terminal domains directly bind to microtubules *in vitro* and whether this function has been conserved in evolution. Bacterially expressed, recombinant POC16/WDR90 DUF667 domains from seven different species were purified and their microtubule interaction ability was assessed using a standard microtubule-pelleting assay (Fig. S1A and Fig. 2C). We found that the POC16/WDR90 DUF667 domain directly binds to microtubules *in vitro*. This interaction was further confirmed using negative staining electron microscopy, where we could observe recombinant WDR90-N localizing on *in vitro* polymerized microtubules (Fig. 2E).

We next investigated whether POC16/WDR90 could also interact with free tubulin dimers, considering that closure of the inner junction between the A and B microtubules necessitates two microtubule/tubulin-binding sites as recently reported for FAP20 (*23*). We observed that all POC16/WDR90 orthologs directly interact with tubulin dimers, generating oligomers that pellet under centrifugation (Fig. 2D). We then tested whether the DUF667 domain could still interact with tubulin once bound to microtubules. We subsequently incubated either

WDR90-N or crPOC16(1-295) pre-complexed with microtubules with an excess of free tubulin and analyzed their structural organization by electron microscopy (Fig. 2E, F and Fig. S3F, G). We observed an additional level of decoration due to the simultaneous complexion of the DUF667 domains with tubulin and microtubules (Fig. 2E, F and Fig. S3F, G). Furthermore, we revealed a 8.5nm periodical organization of tubulin-WDR90-N oligomers on microtubules (Fig. 2G), similar to the FAP20 decoration observed on the microtubule doublet structure in cryo-EM (*23*).

Based on these results, we concluded that POC16/WDR90 is an evolutionary conserved microtubule/tubulin-interacting protein with the capacity to connect microtubules, a functional prerequisite for an inner junction protein that simultaneously interacts with the A and B microtubules.

We next wondered whether POC16/WDR90 could mediate the interaction between microtubule triplets and the underlying inner scaffold. To this end, we took advantage of the strong cellular microtubule decoration of the inner scaffold component FAM161A in human cells when overexpressed ((*24*), Le Guennec et al. in press), in contrast to GFP-WDR90 (Fig. 2H-K). Concomitant overexpression of both proteins leads to a redistribution of GFP-WDR90 on microtubules, suggesting that FAM161A and WDR90 are part of the same molecular complex (Fig. 2L, M). We also observed that GFP-WDR90 co-localizes with mCherry-POC5 when co-expressed and that both redistribute to small and large condensates within the cell, possibly reflecting an interaction (Fig. 2N-Q). As expected, we observed centriolar co-localization of GFP-WDR90 with the two overexpressed inner scaffold proteins.

Taken together, these data demonstrate that WDR90 is a microtubule/tubulin-binding protein that localizes to the central core region of the centriolar microtubule wall. Moreover, we

found that WDR90 interacts with inner scaffold components, suggesting that WDR90 might bridge the centriolar microtubule wall with the underlying inner scaffold structure.

WDR90 is recruited in G2 during centriole core elongation

We next assessed whether WDR90 recruitment at centrioles is correlated with the appearance of inner scaffold proteins during centriole biogenesis. Centrioles duplicate only once per cell cycle during S phase, with the appearance of one procentriole orthogonally to each of the two mother centrioles. Procentrioles then elongate during the following G2 phase of the cell cycle, acquiring the inner scaffold protein POC5 that is critical for the formation of the central and distal parts of the nascent procentriole (Azimzadeh et al., 2009). We followed endogenous WDR90 localization across the cell cycle by analyzing synchronized human RPE1 cells fixed at given time points and stained for either Centrin-2 or HsSAS-6, both early protein marker of duplicating centrioles (*10*, *15*) (Fig. 3 and Fig. S4A, B). We found that while Centrin-2 and HsSAS-6 are recruited as expected early on during procentriole formation in S phase, WDR90 starts appearing only in early G2 when procentriole elongation starts (Fig. 3A-F). Signal intensity analysis over the cell cycle further demonstrates that WDR90 appears on procentrioles in early G2 and reaches full incorporation by the end of G2, similarly to the inner scaffold protein POC5 (*25*) (Fig. 3G, H).

Moreover, we noticed that beside its centriolar distribution, WDR90 localizes also to centriolar satellites, which are macromolecular assemblies of centrosomal proteins scaffolded by the protein PCM1 and involved in centrosomal homeostasis (*26*) (Fig. S4C-H). We tested whether WDR90 satellite localization depends on the satellite protein PCM1 by depleting PCM1 using siRNA and assessing WDR90 distribution. We found that in absence of PCM1, WDR90 is

solely found at centrioles (Fig. S4E-H), demonstrating that WDR90 satellite localization is PCM1-dependent.

Altogether, these data establish that WDR90 is a centriolar and satellite protein that is recruited in G2 of the cell cycle, during procentriole elongation and central core/distal formation, similar to the recruitment of the inner scaffold protein POC5.

WDR90 is important to recruit Centrin-2 and POC5

To better understand the function of WDR90, we analyzed cycling human cells depleted for WDR90 using siRNA and co-labeled WDR90 with either the early centriolar marker Centrin-2 or the protein POC5. As previously shown (*9*), WDR90 siRNA-treated cells showed significantly reduced WDR90 levels at centrosomes in comparison to control cells (Fig. S5A, C). Moreover, we observed an asymmetry in signal reduction at centrioles in WDR90-depleted cells, with only one of two Centrin-2 positive centrioles still associated with WDR90 in G1 and early S-phase (69% compared to 10% in controls) and one of four Centrin-2 positive centrioles in S/G2/M cells (77% compared to 0% in controls, Figure S5B). As the four Centrin-2 positive dots indicate duplicated centrioles, this result suggests that the loss of WDR90 does not result from a duplication failure (Fig. S5B). We postulate that the remaining WDR90 signal possibly corresponds to the mother centriole and that the procentriole is depleted from WDR90 (Fig. S5E), similarly to what has been observed for the protein POC5 (Azimzadeh et al., 2009). We further conclude that WDR90 is stably incorporated into centrioles, in agreement with its possible structural role.

We also noted that the intensity of the Centrin-2 and POC5 signals were markedly reduced upon WDR90 siRNA treatment (Fig. S5D-K). Indeed, we found that only 39% of

WDR90-depleted cells displayed 2 POC5 dots in G1 (negative for HsSAS-6 signal) in contrast to the 86% of control cells with 2 POC5 dots (Fig. S5H). Moreover, 68% of control cells had 2 to 4 POC5 dots in S/G2/M (associated with 2 HsSAS-6 dots) in contrast to 29% in WDR90-depleted condition (Fig. S5H). The HsSAS-6 signal was not affected in WDR90-depleted cells, confirming that initiation of the centriole duplication process is not impaired under this condition (Fig. S5G, J, L). Similarly, the fluorescence intensity of the distal centriole cap protein CP110 was not changed under WDR90-depletion in contrast to the Centrin-2 signal reduction (Fig. S5M-O). These results establish that the localization of Centrin-2 and POC5, two components of the inner scaffold, are affected upon WDR90 depletion in contrast to the proximal protein HsSAS-6 and distal cap protein CP110.

To ascertain this phenotype, we generated a stable cell line expressing a siRNA-resistant version of WDR90 fused to GFP in its N-terminus. We found that expression of GFP-WDR90RR significantly rescued the loss of Centrin-2 and POC5 at centrioles (Fig. 3I- L).

Taken together, these results indicate that the depletion of WDR90 leads to a decrease in Centrin-2 and POC5 localization at centrioles but does not affect the initiation of centriole duplication nor the recruitment of the distal cap protein CP110.

Chlamydomonas POC16 is crucial to maintain centriole core integrity

To investigate the structural role of POC16/WDR90 proteins on centrioles, we initially turned to *Chlamydomonas reinhardtii poc16m504* mutant, which we previously reported to display flagella defects with 80% of mutant cells bearing 0, 1 or impaired flagella (Fig. S6A-C) (*9*). We confirmed, by performing immunofluorescence analysis of wild-type and *poc16m504* *Chlamydomonas* cells co-stained for POC16 and tubulin, that the overall POC16 levels at

centrioles were reduced (Fig. 4A, B). Moreover, we noticed that 52% of *poc16m504* centrioles had only one POC16 dot and 25% had none as compared to the 2 POC16 dots in the wild-type (Fig. 4C). In contrast, by staining for the cartwheel component Bld12 (*11*), we found that the fluorescent signal was similar to wild-type in this background, suggesting that the proximal region of the centriole is not affected (Fig. S6D-F).

To assess whether the ultrastructure and in particular the central core region of centrioles in *poc16m504* cells was defective, we analyzed this mutant using electron microscopy of resin-embedded specimens (Fig. 4D-H). We first noticed that the *poc16m504* mutant displayed shorter centrioles with an average length of 370 nm (+/- 7 nm) compared to 460 nm (+/- 9 nm) in the wild type (Fig. 4D, E). Moreover, we found that the stellate fibers present in the transition zone of wild-type centrioles (Fig. 4D, white star) (*27*), are ectopically localized to the central core region of *poc16m504* mutants in 46% of the cases (Fig. 4D, F-H, red star). This additional localization of stellate fibers has previously been described for the δ-tubulin mutant *uni*-3, which also displays defective microtubule triplets (*28*). However, in contrast to *uni-3*, we noted that microtubule triplets were apparently not affected in the *poc16m504* mutant (Fig. 4G).

In addition, we observed a loss of the inner scaffold structure in comparison to wild-type centrioles, which normally appears as a circular line in electron micrographs (*29*) and which is missing in the *poc16m504* mutant (Fig. 4G, arrows of insets). This suggests either that the loss of the inner scaffold allows for the ectopic localization of the stellate fibers within the central core region of centrioles, or that the presence of the stellate fibers impairs the structure of the inner scaffold. Furthermore, in one instance we observe a centriole with a broken microtubule wall at the level of the central core region, suggestive of centriole fracture (Fig. 4H, arrow).

To better characterize this phenotype, we turned to U-ExM that allows visualization of centrioles ultrastructure in a more quantitative manner in the context of the whole organism (*13*). While the procentrioles looked intact, confirming that proximal assembly initiation is not affected in this mutant, 55% of the *poc16m504* mutants displayed defective mature centrioles compared to wild type (Fig. 4I-K and Fig. S6G). We notably observed incomplete mature centrioles lacking the entire central and distal parts (Fig. 4I, J and Fig. S6G, H). Moreover, consistent with our electron microscopy analysis, quantification of mature centrioles in this mutant demonstrated that intact centrioles are shorter (Fig. 5L).

Altogether, these results demonstrate that the inner scaffold structure of the central core region of *poc16m504* mutants is destabilized, highlighting the role of POC16 in maintaining the structural integrity of the microtubule wall in this region of the centriole.

WDR90 depletion leads to a loss of inner scaffold components and to centriole fracture

Based on the above findings, we wondered whether WDR90 depletion might lead to a loss of all inner scaffold components as well as to a centriole architecture destabilization. We tested this hypothesis by analyzing centrioles from WDR90-depleted cells using U-ExM (Fig. 5). As expected, we observed a strong reduction of WDR90 at centrioles, with a reminiscent asymmetrical signal in one of the two mature centrioles (Fig. 5A, B). Unexpectedly, we found that WDR90-depleted centrioles exhibited a slight tubulin signal increase (502 nm +/- 65 compared to 434 nm +/- 58 in controls), indicative of a defect in centriole length regulation (Fig. 5C).

Prompted by the revealed connection between WDR90 and some inner scaffold proteins, we next analyzed whether the localization of the four described inner scaffold components

POC1B, FAM161A, POC5 and Centrin-2 would be affected in WDR90-depleted cells. We found that the localization of these four proteins in the central core region of centrioles was markedly reduced in WDR90-depleted centrioles (Fig. 5D, E). Instead of covering ~60% of the entire centriolar lumen, we only observed a ~20% remaining belt, positive for inner scaffold components at the proximal extremity of the core region (Fig. 5E, F and Fig. S7A, B), suggesting that their initial recruitment may not be entirely affected. Another possibility would be that the incomplete depletion of WDR90 would allow partial localization of inner scaffold components. It should also be noted that Centrin-2, which displays a central core and an additional distal tip decoration (Le Guennec et al, in press), was affected specifically in its inner core distribution (Fig. 6D, arrow, Fig. S7A, B).

The discovery of the inner scaffold within the centriole led to the hypothesis that this structure is important for microtubule triplet cohesion and thus overall centriole integrity (Le Guennec et al, in press). Remarkably, we found that upon WDR90 depletion, 10% of cells had their centriolar microtubule wall broken, indicative of fracture and loss of centriole integrity (15 out of 150 centrioles, Fig. 6G, H, Movies S1 and S2). The break occurred mainly above the remaining belt of inner scaffold components, possibly reflecting a weakened microtubule wall in the central and distal region of the centriole (Fig. 6G). We also noticed that the perfect cylindrical shape (defined as roundness) of the centriolar microtubule wall was affected with clear ovoid-shaped or opened centrioles, illustrating that loss of the inner scaffold leads to disturbance of the characteristic centriolar architecture (Fig. 6H, Fig. S7C and Movies S1, S2).

Collectively, these data demonstrate that WDR90 is crucial to ensure inner core protein localization within the centriole, to maintain microtubule wall integrity and overall centriole roundness and stability (Fig. 6I).

Discussion

What maintains centriole barrel cohesion and roundness is a fundamental open question. Centrioles experience various forces, while performing their functions in cell division or cilia beating, that they must resist (*8*, *30*, *31*). Centrioles are microtubule barrel structures held together by the A-C linker at their proximal region and a recently discovered inner scaffold in the central/distal region (Le Guennec et al, in press). The presence of such an extended scaffold covering 70% of the centriolar length has led to the hypothesis that this structure is important for maintaining centriole cohesion (Le Guennec et al, in press). Our work demonstrates that POC16/WDR90 family proteins, which are important for cilia and flagella formation, constitute an evolutionary conserved central core microtubule triplet component that is essential for maintaining the inner centriolar scaffold. Their depletions lead to centriole destabilization by impairment of microtubule triplet cohesion, microtubule triplet breakage and loss of their canonical circular shape, thus revealing the crucial function of the inner scaffold.

We first demonstrate that POC16/WDR90 is a component of the microtubule triplet restricted to the central core region. In addition and based on the sequence and structural similarity to the DUF667 domain of FAP20 that composes the inner junction in flagella, we propose that POC16/WDR90 localizes at the inner junction of the A and B microtubule of the centriolar microtubule triplet. In POC16/WDR90, this DUF667 domain is followed by a WD40 domain sharing a homology with the flagellar inner B microtubule protein FAP52/WDR16 (*21*) leading us to postulate that the WD40 domains might also be located inside the B microtubule. However, whether this is the case remains to be addressed in future studies.

Our work further demonstrates that WDR90 is recruited to centrioles in G2 phase of the cell cycle concomitant with centriole elongation and inner central core assembly. We found that WDR90 depletion does not impair centriole duplication nor microtubule wall assembly, as noted by the presence of the proximal marker HsSAS-6 and the distal cap CP110. In stark contrast, WDR90 depletion leads to a strong reduction of inner scaffold components at centrioles, leading to centriole fracture.

Although several examples of centriole cohesion loss have been demonstrated in the past, the molecular mechanisms of centriole disruption are not understood. For instance, Delta- and Epsilon-tubulin null human mutant cells were shown to lack microtubule triplets and have thus unstable centrioles that do not persist to the next cell cycle (*32*). Remarkably, these centrioles can elongate with a proper recruitment of the cartwheel component HsSAS-6 and the distal marker CP110 but fails to recruit POC5, a result that is similar to our findings with WDR90 depleted cells. As Delta- and Epsilon-tubulin null human mutant cells can solely assemble microtubule singlets (*32*), we speculate that WDR90 might not be recruited in these centrioles, as the A microtubule and B microtubule inner junction would be missing. As a consequence, the inner scaffold proteins, such as POC5, will not be recruited, leading to the observed futile cycle of centriole formation and disintegration (*32*). It would therefore be interesting to study the presence of WDR90 in these null mutants as well as the other components of the inner scaffold in the future.

Our work also established that POC16 and WDR90 depletion affects centriole length both in *Chlamydomonas reinhardtii* and human cells. While we observed shorter centrioles in *poc16m504* mutants and the opposite, longer centrioles, in WDR90-depleted cells, these results emphasize the role of POC16/WDR90 in overall centriole length regulation and suggest an

unexpected role of the inner scaffold structure in centriole length control. The observed discrepancy between the two phenotypes could arise from species difference or from the fact that we analyzed a mutant (truncated protein) in the case of POC16 versus an RNAi-mediated depletion in the case of WDR90. Regardless, it would be of great interest to understand how the absence of the inner scaffold can affect the length of the centriole without affecting distal markers such as CP110, which remains unchanged in our experiments. It is very likely that the concomitant elongation of the centriole with the appearance of inner scaffold components in G2 can act on the final length of this organelle.

Given the importance of centriole cohesion in enabling the proper execution of several diverse cellular processes, our work provides new fundamental insights into the architecture of the centriole, establishing a structural basis for centriole cohesion and the severe phenotypes that arise when this cohesion is lost.

References and Notes:

1. P. T. Conduit, A. Wainman, J. W. Raff, Centrosome function and assembly in animal cells. *Nat. Rev. Mol. Cell Biol.* **16**, 611–624 (2015).
2. M. Bornens, The centrosome in cells and organisms. *Science*. **335**, 422–6 (2012).
3. H. Ishikawa, W. F. Marshall, Ciliogenesis: Building the cell's antenna. *Nat. Rev. Mol. Cell Biol.* **12**, 222–234 (2011).
4. D. K. Breslow, A. J. Holland, Mechanism and Regulation of Centriole and Cilium Biogenesis. *Annu. Rev. Biochem.* **88**, 691–724 (2019).
5. E. A. Nigg, J. W. Raff, Centrioles, centrosomes, and cilia in health and disease. *Cell*. **139**, 663–678 (2009).
6. E. A. Nigg, A. J. Holland, Once and only once: Mechanisms of centriole duplication and

their deregulation in diseases. *Nat. Rev. Mol. Cell Biol.* **19**, 297–312 (2018).

7. P. Gönczy, Centrosomes and cancer: revisiting a long-standing relationship. *Nat. Rev. Cancer*. **15**, 639–52 (2015).

8. G. Marteil, A. Guerrero, A. F. Vieira, B. P. De Almeida, P. Machado, S. Mendonça, M. Mesquita, B. Villarreal, I. Fonseca, M. E. Francia, K. Dores, N. P. Martins, S. C. Jana, E. M. Tranfield, N. L. Barbosa-Morais, J. Paredes, D. Pellman, S. A. Godinho, M. Bettencourt-Dias, Over-elongation of centrioles in cancer promotes centriole amplification and chromosome missegregation. *Nat. Commun.* **9** (2018), doi:10.1038/s41467-018-03641-x.

9. V. Hamel, E. Steib, R. Hamelin, F. Armand, S. Borgers, I. Flückiger, C. Busso, N. Olieric, C. O. S. Sorzano, M. O. Steinmetz, P. Guichard, P. Gönczy, Identification of Chlamydomonas Central Core Centriolar Proteins Reveals a Role for Human WDR90 in Ciliogenesis. *Curr. Biol.* **27**, 2486-2498.e6 (2017).

10. P. Strnad, S. Leidel, T. Vinogradova, U. Euteneuer, A. Khodjakov, P. Gönczy, Regulated HsSAS-6 levels ensure formation of a single procentriole per centriole during the centrosome duplication cycle. *Dev. Cell*. **13**, 203–13 (2007).

11. Y. Nakazawa, M. Hiraki, R. Kamiya, M. Hirono, SAS-6 is a cartwheel protein that establishes the 9-fold symmetry of the centriole. *Curr. Biol.* **17**, 2169–2174 (2007).

12. B. E. Tanos, H.-J. Yang, R. Soni, W.-J. Wang, F. P. Macaluso, J. M. Asara, M.-F. B. Tsou, Centriole distal appendages promote membrane docking, leading to cilia initiation. *Genes Dev.* **27**, 163–8 (2013).

13. D. Gambarotto, F. U. Zwettler, M. Le Guennec, M. Schmidt-cernohorska, D. Fortun, S. Borgers, J. Heine, J. Schloetel, M. Reuss, M. Unser, E. S. Boyden, M. Sauer, V. Hamel, P.

Guichard, Imaging cellular ultrastructures using expansion microscopy (U-ExM). *Nat. Methods*. **16** (2019), doi:10.1038/s41592-018-0238-1.

14. F. Zach, F. Grassmann, T. Langmann, N. Sorusch, U. Wolfrum, H. Stöhr, The retinitis pigmentosa 28 protein FAM161A is a novel ciliary protein involved in intermolecular protein interaction and microtubule association. *Hum. Mol. Genet.* **21**, 4573–4586 (2012).

15. J. Azimzadeh, P. Hergert, A. Delouvée, U. Euteneuer, E. Formstecher, A. Khodjakov, M. Bornens, hPOC5 is a centrin-binding protein required for assembly of full-length centrioles. *J. Cell Biol.* **185**, 101–114 (2009).

16. M. Venoux, X. Tait, R. S. Hames, K. R. Straatman, H. R. Woodland, A. M. Fry, Poc1A and Poc1B act together in human cells to ensure centriole integrity. *J. Cell Sci.* **126**, 163–175 (2013).

17. C. G. Pearson, D. P. S. Osborn, T. H. Giddings, P. L. Beales, M. Winey, Basal body stability and ciliogenesis requires the conserved component Poc1. *J. Cell Biol.* **187**, 905–920 (2009).

18. H. Yanagisawa, G. Mathis, T. Oda, M. Hirono, E. A. Richey, H. Ishikawa, W. F. Marshall, M. Kikkawa, H. Qin, FAP20 is an inner junction protein of doublet microtubules essential for both the planar asymmetrical waveform and stability of flagella in Chlamydomonas. *Mol. Biol. Cell*. **25**, 1472–83 (2014).

19. E. E. Dymek, J. Lin, G. Fu, M. E. Porter, D. Nicastro, E. F. Smith, PACRG and FAP20 form the inner junction of axonemal doublet microtubules and regulate ciliary motility. *Mol. Biol. Cell*. **30**, 1805–1816 (2019).

20. H. A. Yanagisawa, G. Mathis, T. Oda, M. Hirono, E. A. Richey, H. Ishikawa, W. F. Marshall, M. Kikkawa, H. Qin, FAP20 is an inner junction protein of doublet

microtubules essential for both the planar asymmetrical waveform and stability of flagella in Chlamydomonas. *Mol. Biol. Cell*. **25**, 1472–1483 (2014).

21. M. Owa, T. Uchihashi, H. aki Yanagisawa, T. Yamano, H. Iguchi, H. Fukuzawa, K. ichi Wakabayashi, T. Ando, M. Kikkawa, Inner lumen proteins stabilize doublet microtubules in cilia and flagella. *Nat. Commun.* **10**, 1–10 (2019).

22. C. Xu, J. Min, Structure and function of WD40 domain proteins. *Protein {&} cell*. **2**, 202–214 (2011).

23. M. Ma, M. Stoyanova, G. Rademacher, S. K. Dutcher, A. Brown, R. Zhang, Structure of the Decorated Ciliary Doublet Microtubule. *Cell*. **179**, 909-922.e12 (2019).

24. F. Zach, F. Grassmann, T. Langmann, N. Sorusch, U. Wolfrum, H. Stöhr, The retinitis pigmentosa 28 protein FAM161A is a novel ciliary protein involved in intermolecular protein interaction and microtubule association. *Hum. Mol. Genet.* **21**, 4573–4586 (2012).

25. J. Azimzadeh, W. F. Marshall, Building the centriole. *Curr. Biol.* **20**, R816-25 (2010).

26. K. Drew, C. Lee, R. L. Huizar, F. Tu, B. Borgeson, C. D. McWhite, Y. Ma, J. B. Wallingford, E. M. Marcotte, Integration of over 9,000 mass spectrometry experiments builds a global map of human protein complexes. *Mol. Syst. Biol.* **13**, 932 (2017).

27. S. Geimer, M. Melkonian, The ultrastructure of the Chlamydomonas reinhardtii basal apparatus: identification of an early marker of radial asymmetry inherent in the basal body. *J. Cell Sci.* **117**, 2663–74 (2004).

28. E. T. O'Toole, T. H. Giddings, J. R. McIntosh, S. K. Dutcher, Three-dimensional Organization of Basal Bodies from Wild-Type and δ-Tubulin Deletion Strains of Chlamydomonas reinhardtii. *Mol. Biol. Cell*. **14**, 2999–3012 (2003).

29. P. Guichard, V. Hachet, N. Majubu, A. Neves, D. Demurtas, N. Olieric, I. Fluckiger, A.

Yamada, K. Kihara, Y. Nishida, S. Moriya, M. O. Steinmetz, Y. Hongoh, P. Gönczy, Native architecture of the centriole proximal region reveals features underlying its 9-fold radial symmetry. *Curr. Biol.* **23**, 1620–8 (2013).

30. M. Abal, G. Keryer, M. Bornens, Centrioles resist forces applied on centrosomes during G2/M transition. *Biol. Cell*. **97**, 425–434 (2008).

31. J. B. Meehl, B. A. Bayless, T. H. Giddings, C. G. Pearson, M. Winey, Tetrahymena Poc1 ensures proper intertriplet microtubule linkages to maintain basal body integrity. *Mol. Biol. Cell*. **27**, 2394–2403 (2016).

32. J. T. Wang, D. Kong, C. R. Hoerner, J. Loncarek, T. Stearns, Centriole triplet microtubules are required for stable centriole formation and inheritance in human cells. *Elife*. **6**, 1–17 (2017).

Acknowledgments: We thank Michel Bornens, Eloise Lequoy-Bertiaux and Nikolai Klena for critical reading of the manuscript. We thank Dr. Kanh Huy Bui for sharing his cryo-EM map EMD-20858. We thank the BioImaging Center and PFMU at Unige. We thank Juliette Azimzadeh for sharing the construct GFP-WDR90-FL. We thank the PhD Booster of the University of Geneva attributed to E.S. **Funding:** This work is supported by the Swiss National Science Foundation (SNSF) PP00P3_157517 (to P.G.) and 31003A_166608 (to M.O.S.), and by the European research Council ERC ACCENT StG 715289 attributed to Paul Guichard. **Author contributions:** E.S. performed and analyzed all the experiments of the paper except for Figure 2C-D. V.H. and Pa.G. conceived, supervised and designed the project. M.O.S. supervised the biochemical microtubule/tubulin-binding experiments. V.H., Pa.G. and E.S. wrote the manuscript with the input from all authors. D.G. and M.H.L. contributed to U-ExM experiments. C.Z., and N.O. expressed and purified the recombinant proteins used in this study, performed the

experiments presented in Figure 2C-D and generated Figure S1A, B. V.O. (together with N. O.) worked on the POC16 model prediction (Figure S2). S.B. provided technical support for Figure 2. M.L.G. provided cryo-EM maps and helped with U-ExM data analysis. F.K. and A-M.T. provided expertise and help for the work performed in *Paramecium tetraurelia* (Figure S1C).

Competing interests: Authors declare no competing interests. **Data and materials availability:** All data is available in the main text or the supplementary materials.

Supplementary Materials:

Materials and Methods

Figures S1-S7

Tables S1-S7

Movies S1-S2

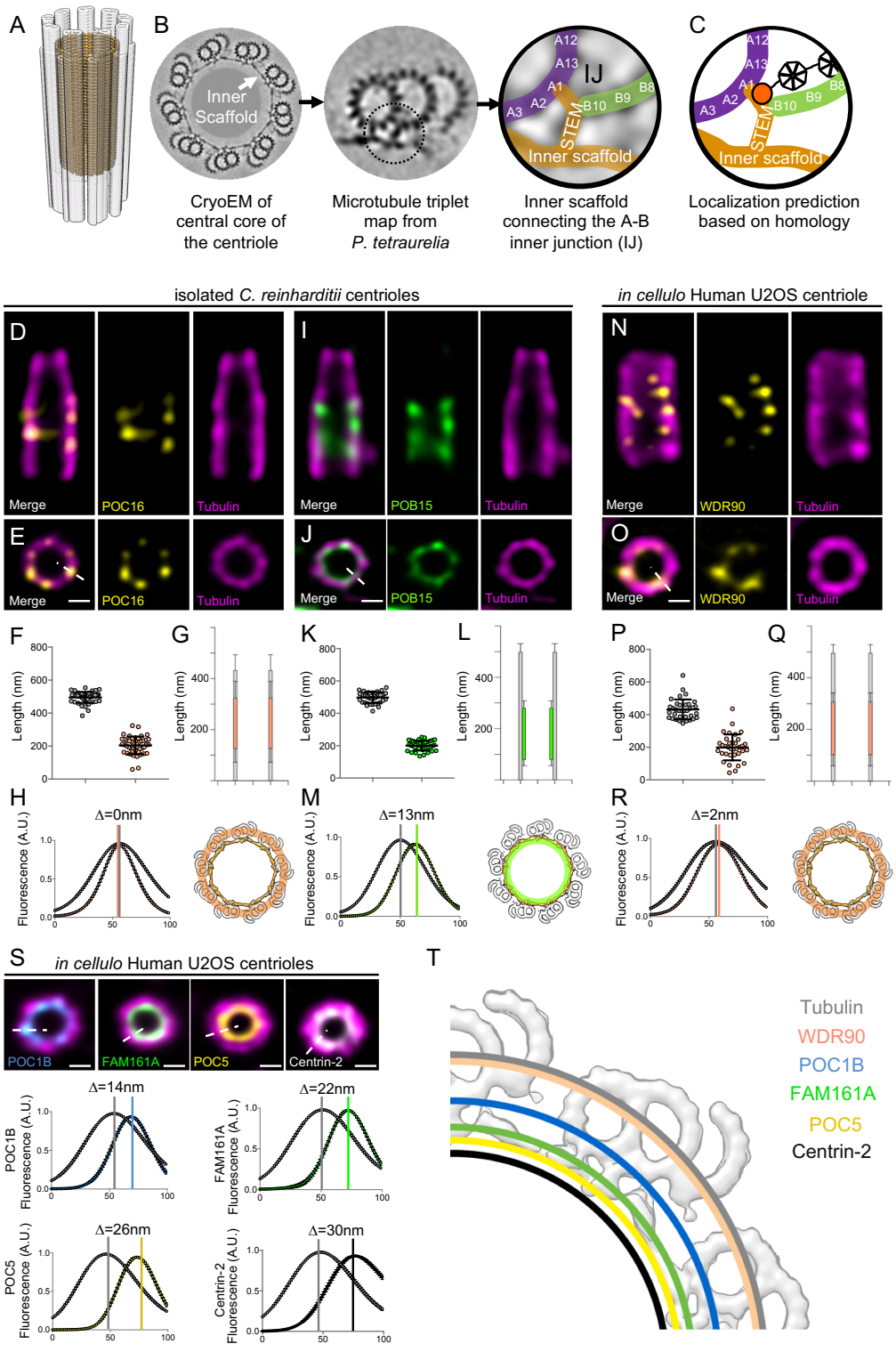

Fig. 1. POC16/WDR90 is a conserved central core microtubule wall component.

(A) 3D representation of a centriole highlighting the centriolar microtubule wall in light grey and the inner scaffold in orange. (B) Cryo-EM image of the central core of *Paramecium tetraurelia* centrioles from which a microtubule triplet map has been generated (Le Guennec et al, in press). Schematic representation of the inner junction (IJ) between A- and B-microtubules connecting the inner scaffold. (C) Schematic localization of POC16/WDR90 proteins within the IJ based on its homology to FAP20. Purple: A-microtubule, green: B microtubule, yellow: inner scaffold and stem and orange: DUF667 domain positioned at the IJ. (D, E) Isolated U-ExM expanded *Chlamydomonas* centriole stained for POC16 (yellow) and tubulin (magenta), lateral (D) and top (E) views. Scale bar: 200nm. (F) Respective lengths of tubulin and POC16 based on D. Average +/- SD: Tubulin: 495nm +/- 33, POC16: 204nm +/- 53, n=46 centrioles from 3 independent experiments. (G) POC16 length coverage and positioning: 41% +/- 11, n=46 centrioles from 3 independent experiments. (H) Tubulin and POC16 fluorescence intensity on microtubule triplets from external to internal based on E (dotted white line). x-value for tubulin maximum intensity peak: 56.63nm, x-value for POC16 maximum intensity peak: 56.63nm, n=92 measurements from 3 independent experiments. Schematic representation of a centriole (top view) based on cryo-EM data highlighting the localization of POC16 (peach) on microtubule triplets. Inner scaffold is in orange. (I, J) Isolated U-ExM expanded *Chlamydomonas* centriole stained for POB15 (green) and tubulin (magenta), lateral (I) and top (J) views. (K) Respective length of tubulin and POB15 based on I. Average +/- SD: tubulin= 497nm +/- 33, POB15= 200nm +/- 30, n=39 centrioles from 3 independent experiments. (L) POB15 length coverage and positioning: 40% +/- 6, n=39 centrioles from 3 independent experiments. (M) Tubulin and POB15 fluorescence intensity along microtubule triplets from external to internal based on J (white dotted line). Scale bar: 200nm. x-value for tubulin max peak: 50nm, x-value for POB15 max peak: 63nm, n=76 measurements

from 3 independent experiments. Schematic representation of a centriole (top view) based on cryo-EM data highlighting the localization of POB15 (green) on microtubule triplets. Inner scaffold is in orange. (N, O) *In cellulo* U-ExM expanded U2OS centriole stained for WDR90 (yellow) and tubulin (magenta), lateral (N) and top (O) views. Scale bar: 200nm (P) Respective lengths of tubulin and WDR90 based on N. Average +/- SD: Tubulin: 432nm +/- 62, WDR90: 200nm +/- 80, n=35 from 3 independent experiments. (Q) WDR90 length coverage and positioning: 46% +/- 17, n=35 from 3 independent experiments. (R) Respective tubulin and WDR90 fluorescence intensity on microtubule triplets from external to internal based on O (white dotted line). x-value for tubulin max peak: 55.31nm, x-value for WDR90 max peak: 57.95nm, n=45 measurements from 3 independent experiments. Schematic representation of a centriole (top view) based on cryo-EM data highlighting the localization of WDR90 (peach) on microtubule triplets. Inner scaffold is in orange. (S) *In cellulo* U-ExM expanded U2OS centrioles stained for POC1B (blue), FAM161A (green), POC5 (yellow) or Centrin-2 (grey) and Tubulin (magenta), top views. Scale bar: 200nm. Tubulin and inner scaffold proteins fluorescence intensity on microtubule triplets from external to internal (dotted white lines in P). All values are given in **Table S1**, n=45 measurements/condition from 3 independent experiments. (T) Position of WDR90 relative to the four inner scaffold components placed on the cryo-EM map of the *Paramecium* central core region (top view) (adapted from Le Guennec et al, in press).

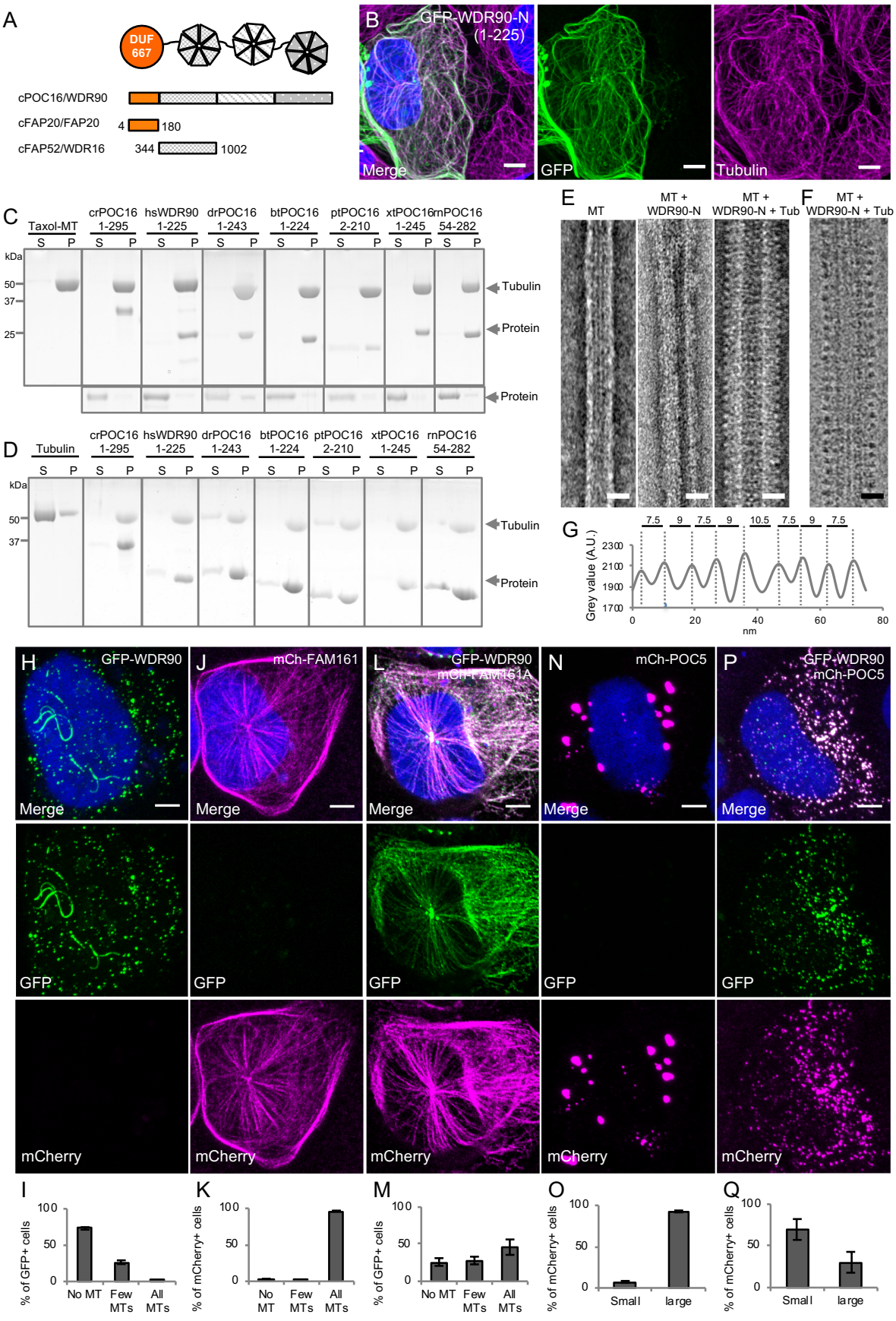
A
DUF 667
cPOC16/WDR90
cFAP20/FAP20
4
180
cFAP52/WDR16
344
1002
B
GFP-WDR90-N (1-225)
Merge
GFP
Tubulin
C
Taxol-MT
crPOC16 1-295
hsWDR90 1-225
drPOC16 1-243
btPOC16 1-224
ptPOC16 2-210
xtPOC16 1-245
rnPOC16 54-282
S P
kDa
50
37
25
Tubulin
Protein
Protein
D
Tubulin
crPOC16 1-295
hsWDR90 1-225
drPOC16 1-243
btPOC16 1-224
ptPOC16 2-210
xtPOC16 1-245
rnPOC16 54-282
kDa
50
37
Tubulin
Protein
E
MT
MT + WDR90-N
MT + WDR90-N + Tub
F
MT + WDR90-N + Tub
G
7.5
9
7.5
9
10.5
7.5
9
7.5
Grey value (A.U.)
2300
2100
1900
1700
0
20
40
60
80
nm
H
GFP-WDR90
Merge
GFP
mCherry
J
mCh-FAM161
Merge
GFP
mCherry
L
GFP-WDR90
mCh-FAM161A
Merge
GFP
mCherry
N
mCh-POC5
Merge
GFP
mCherry
P
GFP-WDR90
mCh-POC5
Merge
GFP
mCherry
I
% of GFP+ cells
100
50
0
No MT
Few MTs
All MTs
K
% of mCherry+ cells
100
50
0
No MT
Few MTs
All MTs
M
% of GFP+ cells
100
50
0
No MT
Few MTs
All MTs
O
% of mCherry+ cells
100
50
0
Small
large
Q
% of mCherry+ cells
100
50
0
Small
large

Fig. 2. WDR90/POC16-DUF667 directly binds both microtubules and tubulin.

(A) Schematic of WDR90/POC16 conservation and homologous domains with the *Chlamydomonas* cilia proteins. FAP20 (DUF667 domain in orange) and FAP52/WDR16 (WD40 repeats in grey). (B) Human U2OS cells transiently overexpressing GFP-WDR90-N (1-225) stained for GFP (green) and tubulin (magenta). Scale bar: 5µm. (C and D) Coomassie-stained SDS-PAGE of pelleting assays performed *in vitro* with taxol-stabilized microtubules (C), and free tubulin (D), in the presence of different recombinant POC16/WDR90-DUF667 protein orthologs (related to Figure S1A, B). The solubility of proteins alone was assessed in parallel to the microtubule-pelleting assay. All tested proteins were soluble under the tested condition (bottom panel). (E) Electron micrographs of negatively stained taxol-stabilized microtubules alone (MT) or subsequently incubated with recombinant WDR90-N (1-225) alone or in combination with tubulin. Scale bar: 25nm (F) Cryo-electron micrograph of taxol-stabilized microtubules subsequently incubated with recombinant WDR90-N (1-225) and tubulin. Scale bar: 25nm (G) Periodicity of complexed WDR90-N (1-225)-tubulin oligomers bound to the microtubule shown in (F). (H, J, L) Human U2OS cells transiently overexpressing GFP-WDR90 (H), mCherry-FAM161A (J), GFP-WDR90 and mCherry-FAM161A (L), fixed and directly imaged in GFP and mCherry channels. Scale bar: 5µm. (I, K, M) Percentage of cells with the following features: (Average +/- SD) GFP-WDR90: no MT decoration: 73% +/- 1, few MT decorated: 26% +/- 2, all MT decorated by GFP-WDR90: 1% +/- 1; mCherry-FAM161A on microtubules: no MT: 2% +/- 1, few MT: 1% +/- 1, all MT: 96% +/- 1; GFP-WDR90 on microtubules in presence of mCherry-FAM161: no MT: 26% +/- 5, few MT: 28% +/- 5, all MT: 46% +/- 10, n=150 cells/condition from 3 independent experiments. (N, P) Human U2OS cells

transiently overexpressing mCherry-POC5 (N), GFP-WDR90 and mCherry-POC5 (P), fixed and directly imaged in GFP and mCherry channels. Scale bar: 5µm. (O, Q) Percentage of cells with the following features: (Average +/- SD): mCherry-POC5 in condensates: small: 7% +/- 1, large: 93% +/- 1, mCherry-POC5 in condensates when co-expressed with GFP-WDR90: small: 70% +/- 12, large: 30 +/- 12, n=150 cells/condition from 3 independent experiments.

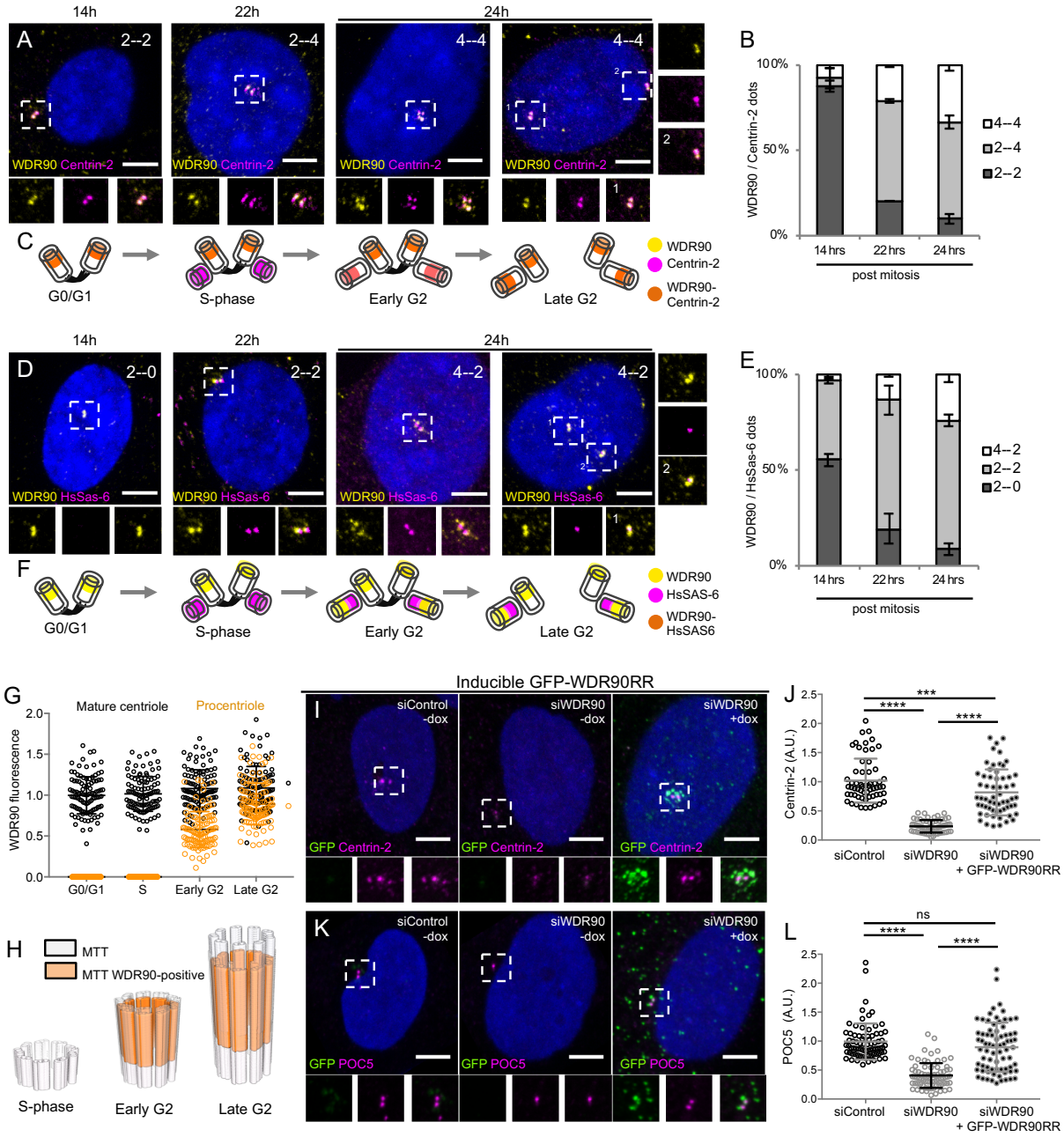

Fig. 3. WDR90 is recruited in G2 and is important for inner scaffold components recruitment to centrioles.

(A) Human RPE1 cells synchronized by mitotic shake-off, fixed at different time points for different cell-cycle stages and stained with WDR90 (yellow) and Centrin-2 (magenta). DNA is in

blue. Dotted white squares correspond to insets. Numbers on the top right indicate corresponding WDR90 and Centrin-2 numbers of dots. Scale bar: 5µm. (B) Percentage of cells with the following numbers of WDR90/Centrin-2 dots based on A, n=300 cells/condition from 3 independent experiments. Average +/- SD: Refer to **Table S2**. (C) Model for WDR90 and Centrin-2 incorporation during centriole biogenesis based on A. (D) Human RPE1 cells synchronized by mitotic shake-off, fixed at different time points for different cell-cycle stages and stained with WDR90 and HsSAS-6. (E) Percentage of cells with the following numbers of WDR90 and HsSAS-6 based on D, n=300 cells/condition from 3 independent experiments. Average +/- SD: refer to **Table S3**. (F) Model for WDR90 and HsSAS-6 incorporation during centriole biogenesis based on D. (G) WDR90 fluorescence intensity at centrioles according to cell cycle progression, n=45 cells/condition from 3 independent experiments. Black fill represents WDR90 at mature centrioles, orange fill represents WDR90 at procentrioles. (H) Schematic representation of WDR90 incorporation during centriole biogenesis according to cell cycle progression based on G. MTT stands for microtubule triplet. (I, K) Human U2OS GFP-WDR90 RNAi-resistant version (GFP-WDR90RR) inducible stable cell line treated with control or *wdr90* siRNA and stained for either GFP and Centrin-2 (I) or GFP and POC5 (K) Scale bar: 5µm. Dotted white squares indicate insets. - and + dox indicates induction of GFP-WDR90RR expression. (J,) Centrosomal Centrin-2 fluorescence intensity based on I, n= 60 cells/condition from 3 independent experiments. Average +/- SEM (A.U.): Control – dox= 1.02 +/- 0.05, siWDR90 – dox= 0.23+/- 0.01, siWDR90 + dox= 0.82 +/- 0.01. Statistical significance assessed by ANOVA. (L) Centrosomal POC5 fluorescence intensity based on K, n= 75 cells/condition from 3 independent experiments. Average +/- SEM (A.U.): Control – dox= 0.99 +/- 0.04,

siWDR90 – dox= 0.41+/- 0.02, siWDR90 + dox= 0.89 +/- 0.05. Statistical significance assessed by ANOVA.

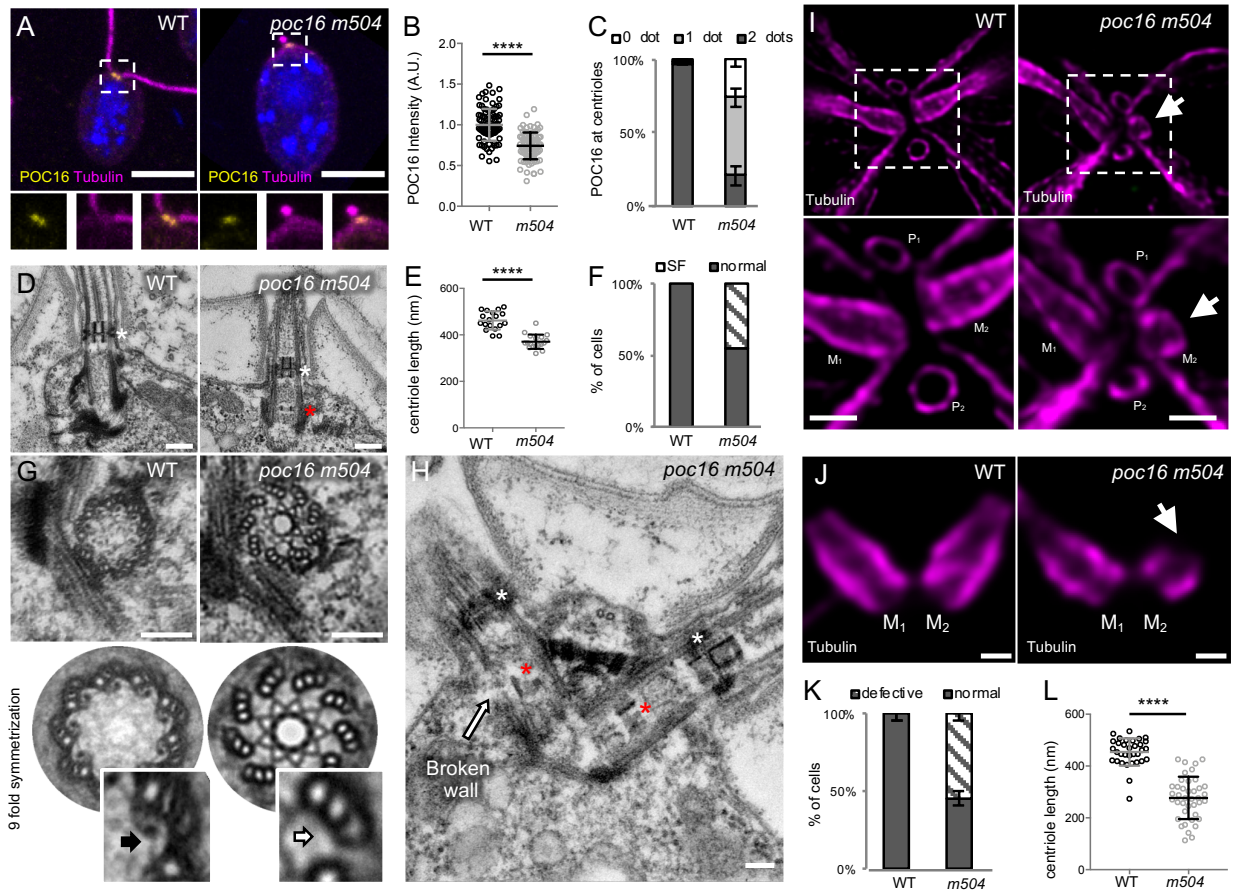

Fig. 4. POC16 mutant lacks the inner scaffold.

(A) Confocal image of *Chlamydomonas* wild-type (WT) and *poc16 m504* mutant stained for tubulin (magenta) and POC16 (yellow), DNA is in blue. Dotted squares correspond to insets. Scale bar: 5µm. (B) POC16 fluorescence intensity based on A, n=90 cells/condition from 3 independent experiments. Average +/- SD: WT: 1+/- 0.2 (A.U.), *poc16m504*: 0.74 +/- 0.2 (A.U.) Normality assessed by Pearson test, Welch T test p< 0.0001. (C) Percentage of cells displaying two, one or no POC16 dots per cell, n=300 cells/condition from 3 independent experiments. Average +/- SD: WT 2 dots: 97% +/- 0.5, 1 dot: 1.3% +/- 1.5, no dot: 1.3% +/- 1.4; *poc16 m504*

2 dots: 20.1% +/- 6.4, 1 dot: 52% +/- 6.1, no dot: 25.2% +/- 4.5. (D) Electron micrograph of *Chlamydomonas* WT and *poc16 m504* revealing the presence of ectopic stellate fibers (SF, white star: normal position in the transition zone; red star: ectopic localization of SF within the central core region of centrioles) inside the lumen of *poc16 m504* centrioles. Scale bar: 250nm (E) Centriole length in WT and *poc16m504* cells, 18 centrioles analyzed in each condition. Average +/- SD: WT= 462 +/- 9nm, *poc16m504*= 371 +/- 7nm. Normality assessed by Pearson test, Welch T test $p< 0.0001$. (F) Percentage of centrioles with ectopic stellate fibers (SF) in WT (0%) and *poc16 m504* (46%), 18 centrioles analyzed in each condition. (G) Electron micrographs of transversal section of *Chlamydomonas* WT (left) and *poc16 m504* (right) centrioles (top panel) and their corresponding circularized and symmetrized version (bottom panel). Top views circularization and symmetrization were performed using CentrioleJ. Arrows indicate the presence (WT, black arrow) and absence (*poc16m504*, white arrow) of the circular inner scaffold. Scale bar: 200nm (H) *poc16 m504* mutant displaying a broken centriolar microtubule wall (white arrow). Note the SF in the transition zone (white star) as well as the ectopic SF (red star) within the central core region of *poc16m504* centrioles. Scale bar: 200nm (I) *In cellulo Chlamydomonas* WT or *poc16m504* centrioles/flagella expanded using U-ExM and stained for tubulin (magenta). M stands for mature centriole and P for procentriole. Arrows points to defective mature centrioles. Scale bar: 200nm (J) *In cellulo Chlamydomonas* WT or *poc16m504* pair of mature centrioles expanded using U-ExM and stained for tubulin (magenta). Arrows point to defective mature centrioles. (K) Percentage of cells with abnormal mature centrioles. Average +/- SD: WT 0% +/- 0, *poc16m504*: 55% +/- 5 from 3 independent experiments. (L) Centriolar length based on J, n= 30 centrioles/condition from 3 independent experiments. Average +/- SD: WT 454nm +/- 53, *poc16m504*: 277nm +/- 82. Mann-Whitney test $p< 0.0001$.

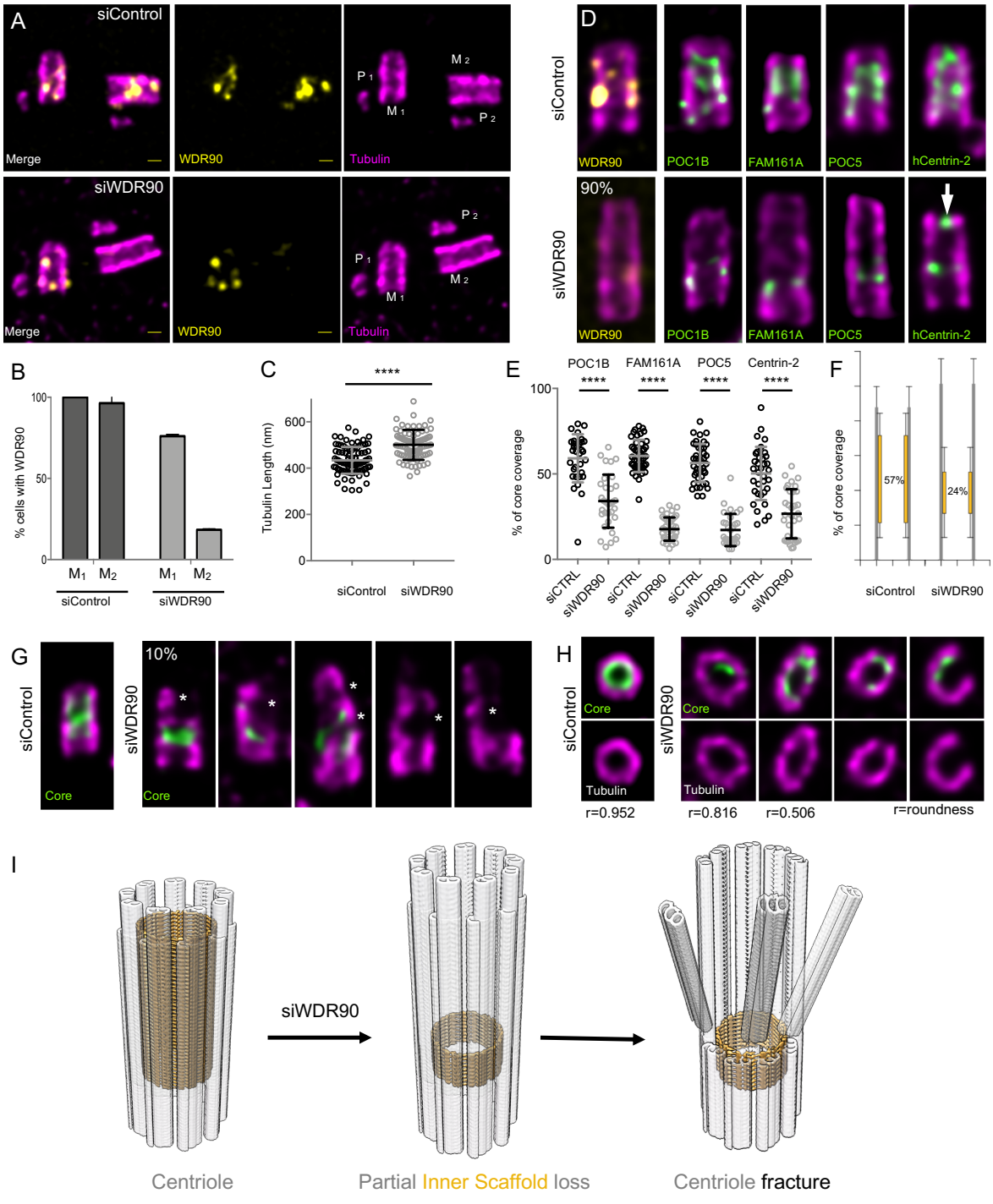

Fig. 5. WDR90 is crucial for centriole integrity.

(A) *In cellulo* U-ExM expanded U2OS centrioles treated with either scramble or *wdr90* siRNA stained for tubulin (magenta) and WDR90 (yellow). Scale bar: 100nm (B) Percentage of cells with WDR90 at mature centrioles based on A, n=90 cells/condition from 3 independent experiments Average +/- SD: siControl= M1: 100% +/- 0, M2: 96% +/- 4.7, siWDR90= M1: 76% +/- 1, M2: 18% +/- 0.6. (C) Tubulin length based on A and D, n=90 centrioles/condition from 3 independent experiments. Average +/- SD: siControl= 434nm +/- 58, siWDR90= 500nm +/- 65. Mann-Whitney $p<0.0001$. (D) *In cellulo* U-ExM expanded U2OS centrioles treated with either scramble or *wdr90* siRNA stained for tubulin (magenta) and WDR90 (yellow) or POC1B, FAM161A, POC5 or Centrin-2 (inner scaffold components: green). (E) Inner scaffold protein length based on D, n>30 centrioles/condition from 3 independent experiments. Average +/- SD: refer to **Table S4**. Statistical significance assessed by ANOVA. (F) Average core length coverage based on E. Average +/- SD: siControl= 57% +/- 13; siWDR90= 24% +/- 14. (G, H) *In cellulo* U-ExM expanded centrioles from U2OS cells treated with scramble or *wdr90* siRNA, stained for tubulin (magenta) and inner scaffold proteins (core, green), displaying microtubule wall fractures (white stars), lateral (G) and top (H) views. Note the loss of roundness of centrioles treated with *wdr90* siRNA. (I) Proposed model of WDR90 function holding microtubule triplets in the central core region of centrioles.

Materials and Methods

Chlamydomonas reinhardti strains

Chlamydomonas strains control wild-type WT (cMJ030, *Chlamydomonas* Resource Center) as well as *poc16 m504* (LMJ.RY0402.069504, *Chlamydomonas* Resource Center) were described and cultured similarly to Hamel et al, 2017.

Human cell lines

Human U2OS and RPE1 p53- cells (gift from Meng-Fu Bryan Tsou) were cultured similarly to Hamel et al, 2017. Cells were grown in DMEM supplemented with GlutaMAX (Life Technology), 10% tetracycline-negative fetal calf serum (life technology), penicillin and streptomycin (100 µg/ml).

To generate inducible episomal U2OS:GFP-WDR90RR cell line, U2OS cells were transfected using Lipofectamine 3000 (Life Technology). Transfected cells were selected for 6 days using 1µg/mL puromycin starting day 2 after transfection. Selected cells were amplified and frozen. For further experiments, U2OS:GFP-WDR90 cell line was grown in the medium specified above supplemented with 1µg/mL puromycin.

Ultrastructure Expansion Microscopie (U-ExM)

In cellulo and isolated *Chlamydomonas* centrioles preparation was previously described (Gambarotto et al., 2019). Coverslips were incubated in 1X AA/FA for 5hrs at 37°C prior to gelation in APS/TEMED/Monomer solution (MS) for 1h at 37°C and denaturation for 30min at 95°C. Specifically, gels were stained for 3hrs at 37°C with primary antibodies against POC16

(1:100) and tubulin (A345) (1:250) or POB15 (1:100) and tubulin (A345) (1:250) (see Le Guennec et al. in press). Gels were washed 3x10min in PBS-T prior to secondary antibodies incubation (1:400) for 3hrs at 37°C and 3x10min washes. A second round of expansion was done 3x150mL ddH20 before imaging.

Human U2OS cells were grown on 12mm coverslips and processed as previously described (see Le Guennec et al. in press). Coverslips were incubated for 5 hours in 2X AA/FA at 37°C. Denaturation was performed for 1h30 at 95° and gels were processed as above. Specifically, staining against WDR90 (1:100) was performed overnight at 37°C.

Imaging was performed on a Leica SP8 microscope using a 63X 1.4NA oil objective with Lightening mode at max resolution to generate deconvolved images. 3D stacks were acquired with 0.12µm z-interval and an x, y pixel size of 35nm.

Cloning, and transient overexpression in Human cells

GFP-WDR90-N(1-225)RR and GFP-WDR90(FL)RR were cloned in the Gateway compatible vector pEBTet-eGFP-GW. Previously generated RNAi-resistant WDR90 DNA (*1*) was used as template for PCR amplification. In brief, inserts were first subcloned in pENTR-Age-AGT using the restriction sites AgeI and XbaI. Second, a Gateway reaction was performed to generate the final expression plasmids pEBTet-GFP-WDR90-N(1-225)RR and pEBTer-GFP-WDR90(FL)RR, which were sequenced verified prior to transfection in human cells.

For transient expression, U2OS cells were transfected using Lipofectamine 3000 (Life Technology). Protein expression was induced using 1µg/mL doxycycline for 48 hours and cells were processed for immunofluorescence analysis.

Cloning of the GFP-WDR90 construct used in Fig. 2 was done as follows: Human WDR90 was cloned by nested RT-PCR using total RNAs extracted from human RPE1 cells. Three different fragments corresponding to aa. 1-578, 579-1138, 1139-1748 of WDR90 (based on Genebank sequence NP_660337) were amplified and cloned separately using the pCR Blunt II Topo system (Thermo Fisher Scientific). The full coding sequence was then reconstituted in pCR Blunt II by two successive cloning steps using internal *Nru* I and *Sal* I, introduced in the PCR primers and designed in order not to modify WDR90 aa sequence. WDR90 coding sequence was then cloned into a modified pEGFP-C1 vector (Clontech) containing *Asc* I and *Pac* I restriction sites.

Immunofluorescence in Human cells

Cells grown on a 15 mm glass coverslips (Menzel Glaser) were pre-extracted for 15sec in PBS supplemented with 0.5% triton prior to iced-cold methanol fixation for 7min. Cells were washed in PBS then incubated in 1% bovine serum albumin (BSA) in PBS-T with primary antibodies against WDR90 (1:250), Centrin-2 (1:500), HsSAS-6 (1:100), PCM1 (1:500), CP110 (1:500), GFP (1:500), mCherry (1:500) or tubulin (1:500). Coverslips were washed in PBS for 30min prior to incubation with secondary antibodies (1:1000) for 1 hour at room temperature, washed again for 30min in PBS and mounted in DAPCO mounting medium containing DAPI (Abcam). Imaging was performed on a Zeiss LSM700 confocal microscope with a PlanApo 63x oil immersion objective (NA 1.4) and optical sections were acquired every 0.33 mm, then projected together using ImageJ.

Cloning and protein purification

The constructs encompassing the predicted DUF667 domain of crPOC16 (Uniprot: A8JAN3), hsWDR90 (Uniprot: Q96KV7), drPOC16 (Uniprot: F1RA29), btPOC16 (Uniref: UPI000572B175), ptPOC16 (Uniprot: A0DK60), xtPOC16 (Uniref: UPI0008473371) and rnPOC16 (Uniref UPI0008473371) were cloned into a pET based expression vector via Gibson assembly (*2*).

All recombinant proteins contained a N-terminal thioredoxin (TrxA) tag, used to enhance the expression level and the solubility of the target protein, followed by a 6xHis tag and a 3C cleavage site.

Protein expression was carried out in *E. coli* BL21 (DE3) competent cells grown in LB media at 37°C to OD_{600} = 0.6 and induced for 16h at 20°C with 1mM IPTG. Cells were subsequently resuspended in lysis buffer (50 mM Hepes pH 8, 500 mM NaCl, 10% v/v glycerol, 10 mM imidazole pH 8, 5 mM β-mercaptoethanol) supplemented with DNase I (Sigma), complete EDTA-free protease inhibitor cocktail (Roche) and lysed by sonication. The supernatant was clarified by centrifugation (18000 rpm, 4˚C, 45 min), filtered and loaded onto a HisTrap HP 5 ml column (GE Healthcare). After extensive washes with wash buffer (50 mM Hepes pH 8, 500 mM NaCl, 10% v/v glycerol, 20 mM imidazole pH 8, 5 mM β-mercaptoethanol), the bound protein was eluted in the wash buffer supplemented with 400 mM imidazole. For crPOC16, hsWDR90, drPOC16 and xtPOC16, a 10 to 400 mM imidazole gradient was required to successfully detach the protein from the column.

The protein-containing fractions were pooled together and dialysed against the lysis buffer at 4˚C for 48 hours in the presence of the 6xHis-3C protease. The tag-free protein was reapplied onto a HisTrap HP 5 ml column (GE Healthcare) to separate the cleaved product from the respective tags and potentially uncleaved protein. The processed proteins were concentrated and further

purified by size exclusion chromatography (Superdex-75 16/60, GE Healthcare) in running buffer (20 mM Tris pH 7.5, 150 mM NaCl, 2 mM DTT). Protein were analysed by Coomasie stained SDS-PAGE and the protein-containing fractions were pooled, concentrated and flash-frozen for storage at -80˚C. All protein concentrations were estimated by UV absorbance at 280 nm.

Microtubule binding assay

Taxol-stabilized microtubules (MTs) were assembled in BRB80 buffer (80 mM PIPES-KOH pH6.8, 1 mM $MgCl_2$, 1 mM EGTA) from pure bovine brain tubulin at 1 mg/mL (Centro de Investigaciones Biológicas, Madrid, Spain). 50 µL of stabilized MTs were incubated with 20µL of protein at 1 mg/mL for 2 hours at room temperature. After centrifugation on a taxol-glycerol cushion (8'000 rpm, 30°C, 20min) the supernatant and the pellet were analyzed by Coomasie stained SDS-PAGE gels. As a control, MTs alone and each protein alone were processed the same way.

Tubulin binding assay

Tubulin at 10 µM was incubated with a slight molar ratio excess of each protein construct (around 15 µM) in MES buffer for 15 min on ice. After centrifugation at 13'000 x g at 4°C for 20 min, the supernatant and the pellet were analyzed by Coomasie stained SDS-PAGE.

***In vitro* microtubules decoration and imaging**

For simple decoration, Taxol-stabilized microtubules were nucleated as described (*3*) and subsequently exposed to recombinant WDR90-N(1-225) in a 1:1 molar ratio for 30min at room

temperature. Five μL of protein complexes solution were blotted on Lacey carbon grids and stained with Uranyl Acetate (2%) for 3 then 30 seconds.

For double decoration, *in vitro* microtubules were incubated with WDR90-N(1-225) in a 1:1 molar ratio for 5min at room temperature prior to addition of 2X free tubulin for 30min at room temperature. Negatively stained grids were prepared as above. Similarly, double decorated microtubules were prepared for cryo-fixation.

Electron micrographs were acquired on a Technai 20 electron microscope (FEI Company) and analyzed using ImageJ.

Displacement assay

U2OS cells were transfected in a 6-well plate using jetPRIME reagent (Polyplus-transfection, cat-114-07) following the manufacturer's instructions, with 2.5μg total DNA of the following combinations: GFP-WDR90 alone, mCherry-FAM161A alone, GFP-WDR90 and mCherry-FAM161A, mCherry-POC5 alone and GFP-WDR90 and mCherry-POC5. The medium was changed 4-6 hours after transfection and expression of the fluorescent fusion proteins was allowed for 24 hours. Cells grown on coverslips were pre-extracted for 15sec in PBS supplemented with 0.5% triton prior to iced-cold methanol fixation for 3min. Coverslips were washed once in PBS, mounted and directly imaged in GFP and mCherry channels.

For quantification, cells were classified as "No MT" when no cytoplasmic microtubule pattern was observed, "Few MT" when only a subset of microtubules were decorated or when microtubules were partially decorated along their length, and "All MT" when we observed total coverage of the cytoplasmic microtubule network.

Mitotic shake off

RPE1 p53- cells were seeded in T300 flasks the day before shake off. Flasks were shaken vigorously to detach mitotic cells collected in medium. Cells were pelleted by centrifugation for 5min at 1000 rpm and suspended in 10nM EdU containing medium prior to seeding in 6 well plates onto 15mm coverslips. Cells were fixed at different time points and processed in parallel for immunofluorescence or FACS analysis.

WDR90 depletion using siRNA

U2OS cells were plated onto 15mm coverslips in a 6-well plate and 10nM silencer select pre-designed siRNA s47097 was transfected using Lipofectamine RNAimax (Thermo Fischer Scientific). Medium was changed 4hrs and 48hrs post-transfection and cells were analyzed 96hrs post-transfection.

In U2OS:GFP-WDR90(FL-RR) stable cell line, RNA-resistant protein expression was induced constantly for 96hrs using 1µg/mL doxycycline.

Immunofluorescence on *Chlamydomonas reinhardti* cells

Chlamydomonas cells were sediment on Poly-D-Lysine coated-12mm coverslips (Menzel Glaser) for 30min prior to 7min fixation in -20°C methanol. Cells were washed in PBS then incubated in 1% bovine serum albumin (BSA) in PBS-T with primary antibodies against POC16 (1:500), Bld12 (1:100) and Tubulin DM1α (1:500) for 1h at room temperature. Coverslips were washed in PBS for 30min prior to incubation with secondary antibodies for 1 hour at room temperature, washed again for 30min in PBS and mounted in DAPCO mounting medium containing DAPI (Abcam).

Imaging was performed on a Zeiss LSM700 confocal microscope with a PlanApo 63x oil immersion objective (NA 1.4) and optical sections were acquired every 0.33 nm, then projected together using ImageJ.

Electron microscopy on *Chlamydomonas reinhardti*

For sample preparation, cells were pelleted for 5min at 500g, fixed in 2.5% glutaraldehyde/TAP 1X for 1h at RT and washed 3x in TAP 1X. Fixed cells were further treated with 2% osmium tetraoxyde in buffer and immersed in a solution of uranyl acetate 0.25% over night to enhance contrast of membranes. The pellets were deshydrated in increasing concentrations of ethanol followed by pure propylene oxide and embedded in Epon resin. Thin sections for electron microscopy were stained with uranyl acetate and lead citrate, and observed in a Technai 20 electron microscope (FEI Company).

Micrographs analyses were performed on ImageJ and GraphPadPrism7.

Symmetrization on top views was performed using CentrioleJ pluggin (https://gonczy-lab.epfl.ch/resources/ressources-centriolej/). The UnwarpJ plugin was required to perform image circularization using the center of the nine A-microtubules as landmark points. A 9-fold symmetrization was then applied to the circularized image. The deformation parameters were adjusted depending on the quality of the original image. For WT: initial deformation → fine, final deformation → fine. For m504: initial deformation→ fine, final deformation→ very fine.

Image analysis

For centrioles counting, immunofluorescences were analyzed on a Leica epifluorescence microcoscope.

For fluorescence intensity, maximal projections were used.

Centrosomal intensities were assessed using an area of 20 pixels on Fiji. Control values were averaged, normalized to 1 and all other values were compared accordingly. Individual values were plotted in GraphPadPrism7.

Centriolar intensities were assessed by individual plot profile on each centrioles pair. Within pairs, the highest maximum fluorescence value (y-axis) was rescaled to 1 and all the other values were normalized to it. Averages were generated and plotted in GraphPad Prism7.

For U-ExM data, length coverage quantification was performed like in Le Guennec et al (in press). The Fiji plot profile tool was used to obtain the fluorescence intensity profile from proximal to distal for tubulin and the core protein from the same line scan.

For top views, a measurement from the exterior to the interior of the centriole was performed on each microtubule triplet displaying a resolved signal for both tubulin and the core protein. For each tubulin fluorescence intensity profile, the highest maximum fluorescence value (y-axis) was rescaled to 1 and all the other values were normalized to it. Averages were generated and plotted in GraphPad Prism7.

Roundness was calculated on perfect top views of centrioles by connecting tubulin peaks on ImageJ.

Statistical analysis

The comparison of two groups was performed using a two-sided Student's t-test or its non parametric correspondent, the Mann-Whitney test, if normality was not granted either because not checked ($n < 10$) or because rejected (D'Agostino and Pearson test). The comparisons of more than two groups were made using one or two ways ANOVAs followed by post-hoc tests

(Holm Sidak's) to identify all the significant group differences. N indicates independent biological replicates from distinct sample. Every experiment, except for resin electron microscopy, was performed at least 3 times independently. Data are all represented as scatter or aligned dot plot with centerline as mean, except for percentages quantifications, which are represented as histogram bars. The graphs with error bars indicate 1 SD (+/-) and the significance level is denoted as usual (*p<0.05, **p<0.01, ***p<0.001, ****p<0.0001). All the statistical analyses were performed using Excel or Prism7 (Graphpad version 7.0a, April 2, 2016).

Protein alignement

The protein sequences were aligned using Clustal Omega and the secondary structure elements were predicted using Phyre 2, PONDR and XtalPred-RF.

3D modelisation

The *Chlamydomonas* POC16 model was prepared using *Phyre2* (Kelley 2015 Nature Protocols) and refined against the FAP20 cryo-EM map EMD_20858 using *phenix.real_space_refine* (Afonine 2018 ActaD). Superposition of the POC16 model excluding flexible loops against FAP20 was done using *COOT* (Emsley 2010 ActaD) and yielded a rmsd value of 1.6 Angs. The figures were prepared using *ChimeraX* (Goddard 2018 Protein Science).

PtPOC16 antibody purification

To generate anti-PtPOC16 antibody, a fragment encoding amino acids 2-210 was used for rabbit immunization (Eurogentec). Antibodies were subsequently affinity-purified over a column of

PtPOC16(2-210) immobilized on Affi-Gel 10 (Bio-Rad Laboratories) and dialyzed against PBS/5% glycerol.

Immunofluorescence in *Paramecium tetraurelia*

Immunofluorescence was performed according to Beisson et al, 2010. Briefly, Paramecia were permeabilized for 5min in 0.5% saponin in PHEM Buffer (PIPES 60mM, HEPES 25mM, EGTA 10mM, 2mM MgCl2 pH 6.9) and fixed in 2% paraformaldehyde (PFA) for 10 min. Cells were washed 3x10min in PHEM-saponin buffer and stained with primary antibodies against POC16 (1:100) and tubulin 1D5 (1:10) for 30min at room temperature. Cells were incubated with secondary antibodies for 20min, washed twice in PHEM-saponin prior to a last wash in TBST-BSA supplemented with Hoescht 2mg/mL.

Imaging was performed on a Zeiss LSM700 confocal microscope with a PlanApo 40x oil immersion objective (NA 1.4) and optical sections were acquired every 0.33 mm, then projected together using ImageJ.

Human cells cold shock treatment

U2OS cells grown on 15mm coverslips and transiently overexpressing mCherry-WDR90-N(1-225)RR for 24hrs were placed in 4°C PBS for an hour on ice and fixed in -20°C methanol. Coverslips were processed for immunofluorescence using primary antibodies against mCherry (1:500) and anti-tubulin DM1α (1:1000).

***In vitro* crPOC16 microtubule decoration**

In vitro stabilized Taxol-microtubules were prepared in MES-BRB80 derived buffer in contrast to K-PIPES-BRB80 to allow crPOC16(1-295) protein solubility. Samples were then processed similarly to WDR90-N(1-225).

FACS analysis

Cells were processed similarly to Macheret et al 2018. Post-mitotic cells were washed 2x with PBS then permeabilized and treated with Click-EdU-Alexa 647 (Roth - 7783.1) according to manufacturer's instruction. Genomic DNA was stained with propidium iodide (Sigma, Cat. No. 81845) in combination with RNase (Roche, Cat. No. 11119915001). EdU-DNA content profiles were acquired by flow cytometry (Gallios, Beckman Coulter) to assess the percentage of cells that entered S phase in each condition at each time point.

PCM1 depletion using siRNA

U2OS cells were plated onto 15mm coverslips in a 6 well plate and 20nM silencer select pre-designed siRNA ADCSU9L was transfected using Lipofectamine RNAimax (Thermo Fischer Scientific). Medium was changed 4hrs post-transfection and cells were analyzed 48 hours post-transfection.

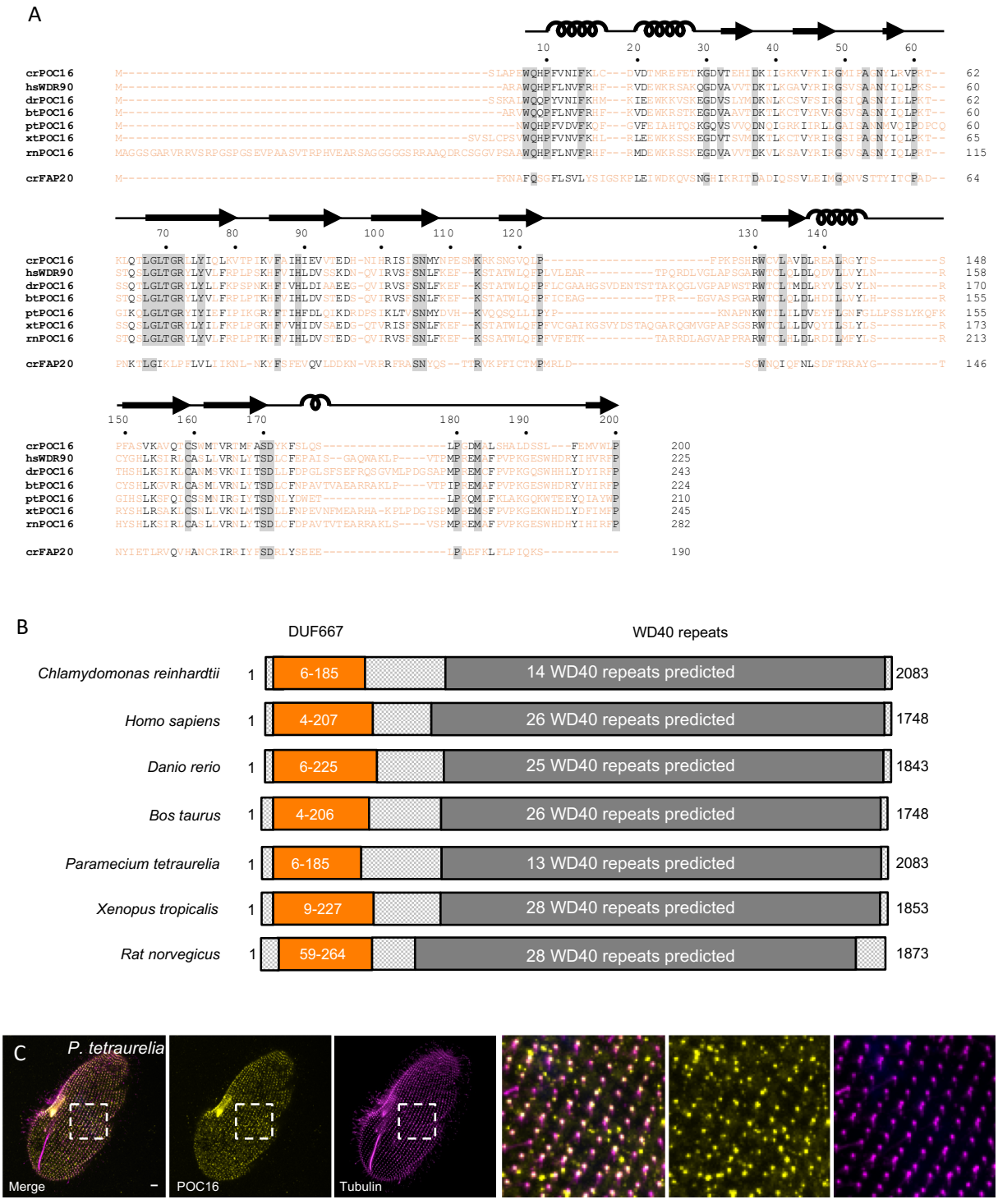

Fig. S1. POC16 conservation across species.

(A) POC16 orthologs DUF667 domain amino acids sequence alignment from 7 different species: *Chlamydomonas reinhardtii* crPOC16(1-200); *Homo sapiens* hsWDR90(1-225), *Danio rerio*

drPOC16(1-243), *Bos taurus* btPOC16(1-224), *Paramecium tetraurelia* ptPOC16(1-210), *Xenopus tropicalis* xtPOC16(1-245) and *Rat norvegicus* rtPOC16(1-282). Note also below the alignment with *Chlamydomonas reinhardtii* crFAP20. The secondary structures α-helices and β-strand are indicated on top of the amino acid sequences. (B) POC16 orthologs domain mapping and conservation. Orange: DUF667 domain. Dark grey: WD40 repeats. (C) *Paramecium tetraurelia* cell fixed and stained for ptPOC16 (yellow) and tubulin (1D5) (magenta), showing that ptPOC16 is a centriolar component. Scale bare: 10μm.

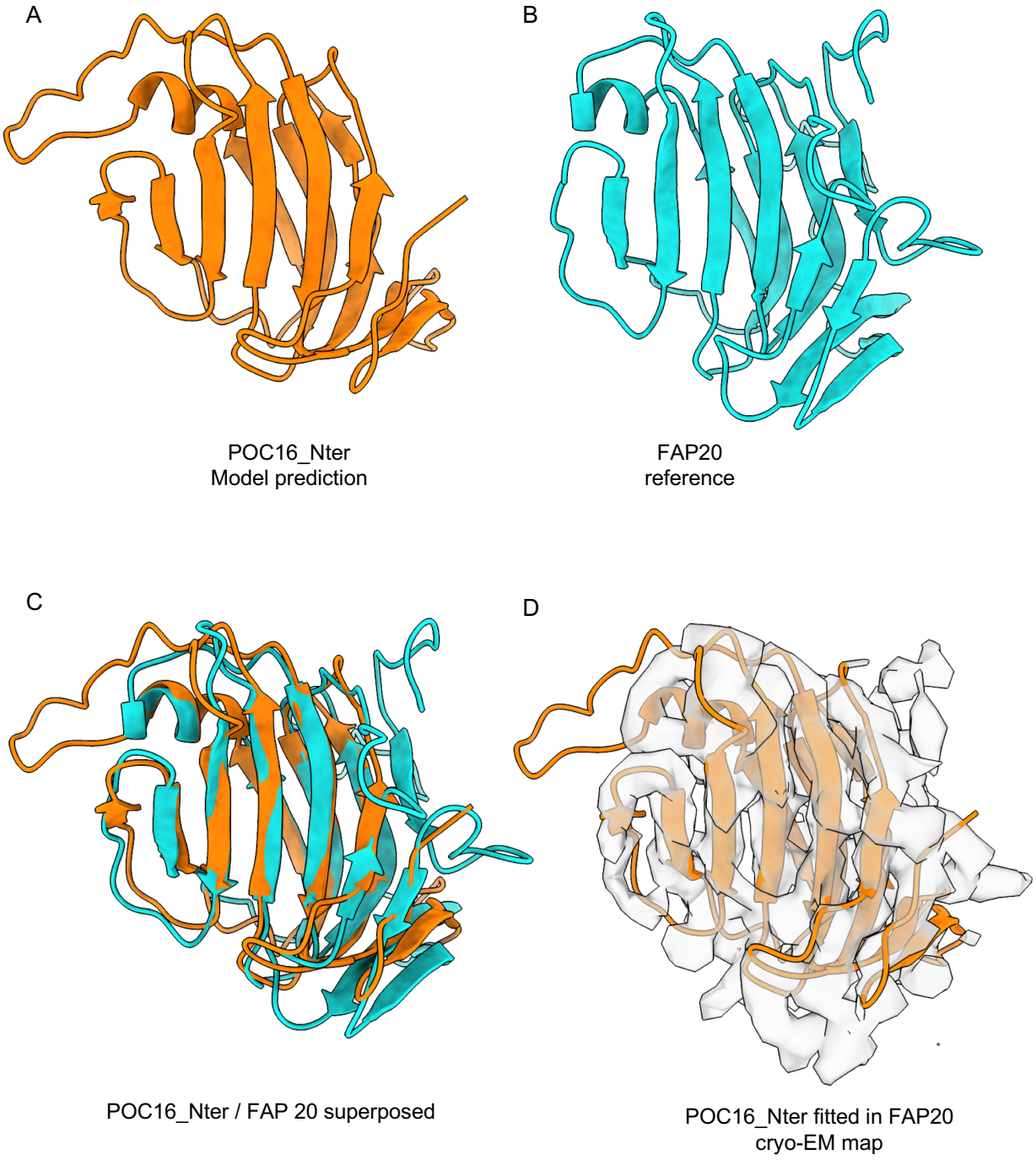

Fig. S2. Model prediction of POC16 Nter.

(A) POC16 3D model and (B) FAP20 reference structure model (*4*). (C) Fitting of POC16 against FAP20 yielding a rmsd value of 1.6 Angs. (D) Fitting of the POC16 model excluding the flexible loops in the FAP20 cryo-EM electron density map.

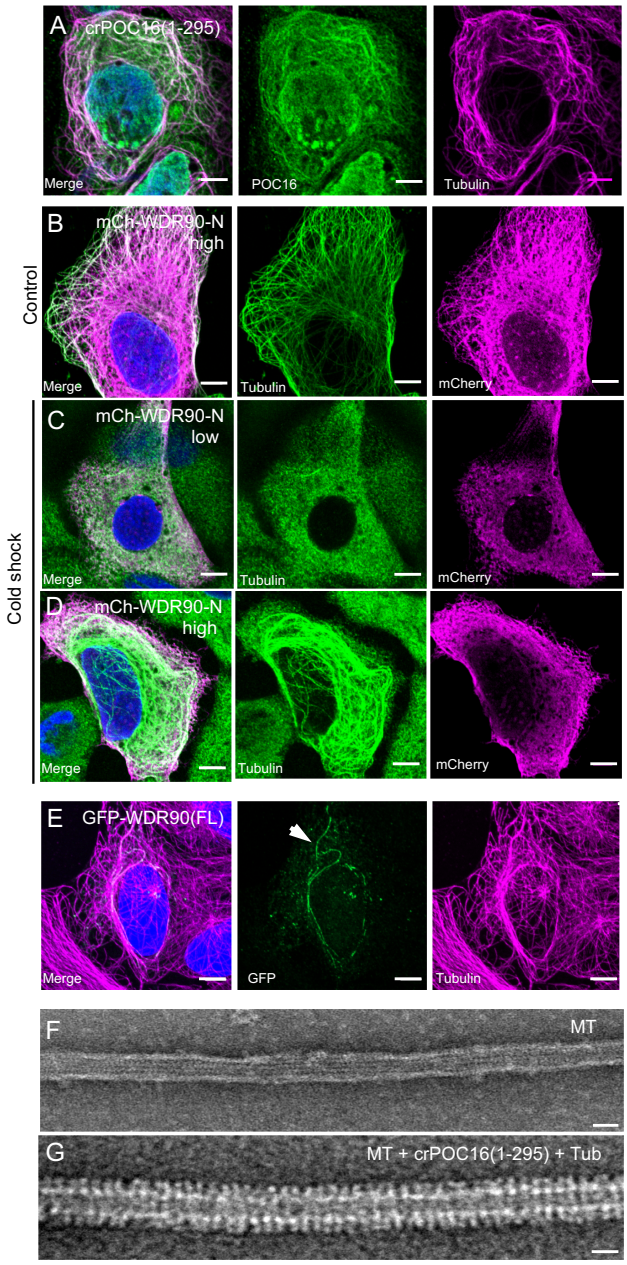

Fig. S3. POC16 and WDR90 bind microtubules.

(A) Human U2OS cells transiently overexpressing GFP-crPOC16(1-295) stained for POC16 (green) and tubulin (magenta). Scale bars for panels A-E: 5µm. (B) Human U2OS cells transiently overexpressing at high level mCherry-WDR90-N(1-225), fixed in control condition

and stained for tubulin (green) and mCherry (magenta). (C) Human U2OS cells transiently overexpressing at low level mCherry-WDR90-N(1-225), fixed after 1h of cold shock treatment and stained for tubulin (green) and mCherry (magenta). (D) Human U2OS cells transiently overexpressing at high level mCherry-WDR90-N(1-225), fixed after 1h of cold shock treatment and stained for tubulin (green) and mCherry (magenta). (E) Human U2OS cells transiently overexpressing GFP-WDR90(FL) stained for GFP (green) and tubulin (magenta). Arrow indicates WDR90-decorated microtubules. (F) Electron micrograph of negatively stained *in vitro* taxol-stabilized microtubules. Scale bar: 25nm (G) Electron micrograph of negatively stained *in vitro* taxol-stabilized microtubules incubated with recombinant POC16(1-295) and free tubulin. Scale bar: 25nm.

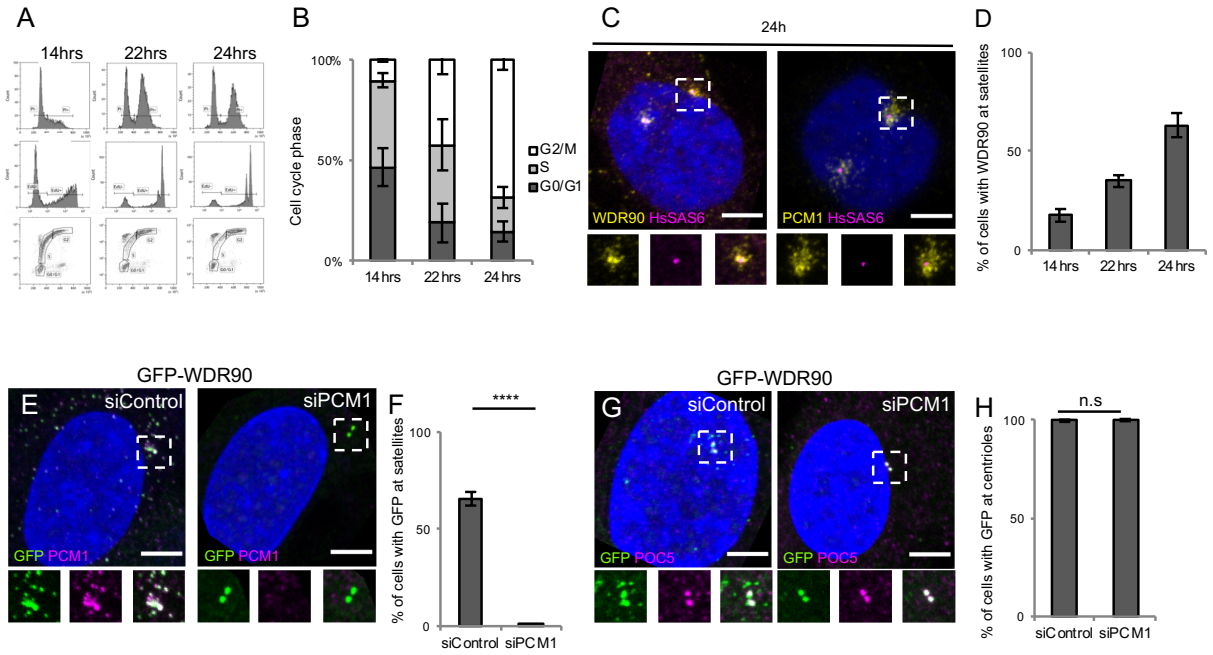

Fig. S4. WDR90 is a satellite and centriolar protein.

(A) FACS profiles of RPE1 p53- cells at different time point post mitotic shake-off, plotted based on propidium iodide (PI) and 5-ethynyl-2′-deoxyuridine (EdU) content. Related to Fig. 5(A-E). (B) Percentage of cells in G0/G1, S or G2/M phase based on A, n=25000 cells/condition from 3 independent experiments. Average +/- SD: Refers to **Table S5**. (C) Human RPE1p53- fixed 24 hours post mitosis and stained for WDR90 (yellow) and HsSAS-6 (magenta) or PCM1 (yellow) and HsSAS-6 (magenta). DNA is in blue. Scale bar: 5µm. Dotted white squares indicate insets. (D) Percentage of cells displaying WDR90 satellite pattern based on C, n=150 cells/condition from 3 independent experiments. Average +/- SD: 14hrs: 18% +/- 3, 22hrs: 35% +/- 3, 24hrs: 63% +/- 6. (E) Human U2OS cells treated with scramble or *pcm1* siRNA and stained for GFP and PCM1. Scale bar: 5µm. Dotted white squares indicate insets (F) Percentage of cells with GFP-WDR90 at satellites based on F, n=300 cells/condition from 3 independent experiments Average +/- SD: siControl: 66% +/- 4, siPCM1: 1% +/- 1. Welch T-test $p<0.0001$.

(G) Human U2OS cells treated with scramble or *pcm1* siRNA and stained for GFP and POC5. Scale bar: 5µm. Dotted white squares indicate insets. (H) Percentage of cells with GFP-WDR90 at centrioles based on H, n=300 cells/condition from 3 independent experiments Average +/- SD: siControl: 99% +/- 1, siPCM1: 100% +/- 1. Welch T-test p=0.5185.

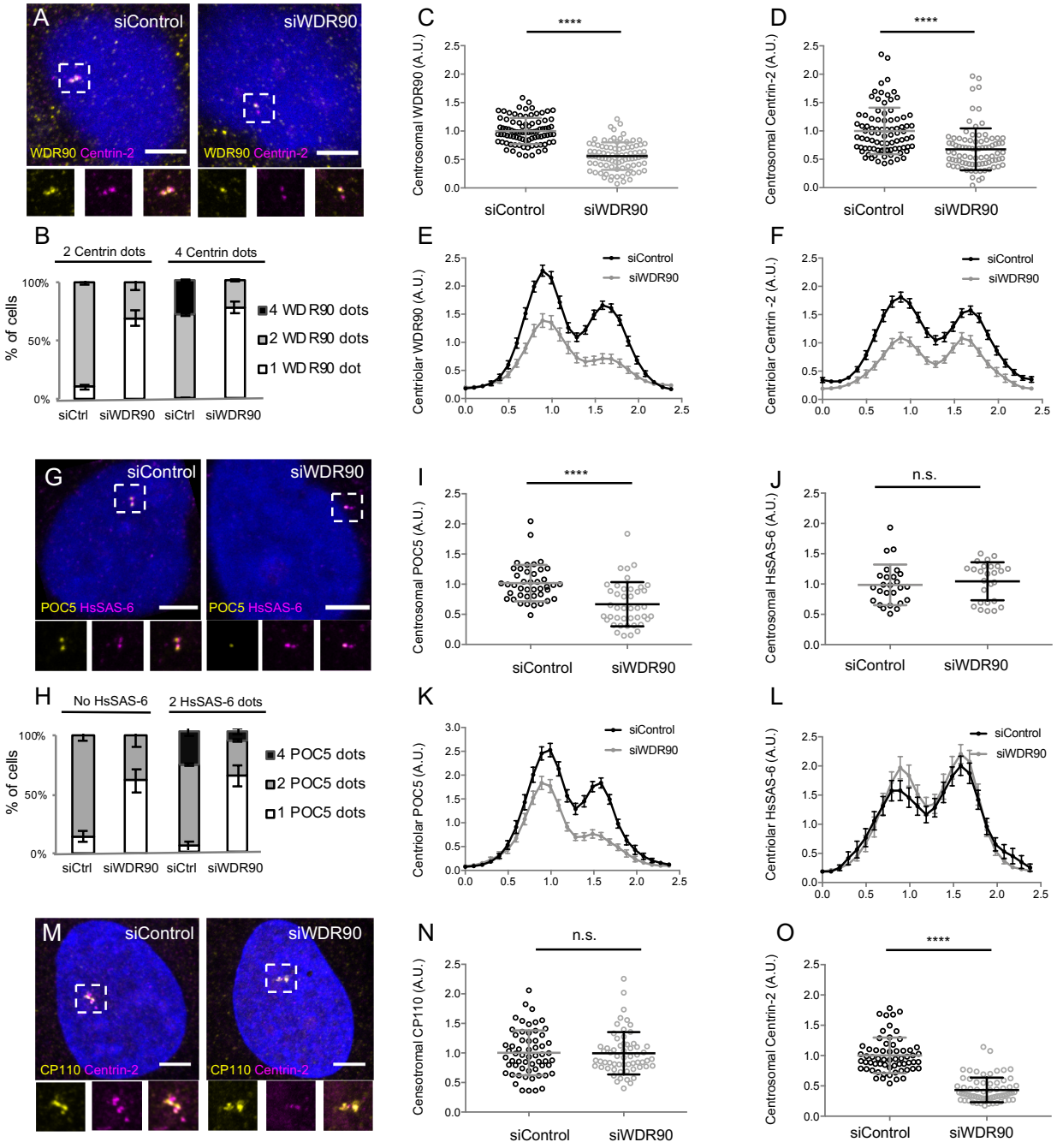

Fig. S5. Depletion of WDR90 impairs Centrin-2 and POC5 localization at centrioles.

(A) Human U2OS cell treated with either scramble or *wdr90* siRNA and stained for WDR90 (yellow) and Centrin-2 (magenta). DNA is in blue. Dotted white squares indicate insets. Scale bar: 5µm. (B) Percentage of cells with the following number of WDR90 dots according to the

number of Centrin-2 dots per cell based on A, n=150 cells/condition from 3 independent experiments. Average +/- SD: Refer to **Table S6** (C) WDR90 centrosomal intensity based on A, n=90 cells/condition from 3 independent experiments. Average +/- SD: siControl: 1 +/- 0.2 (A.U.), siWDR90: 0.56 +/- 0.2 (A.U.). Normality assessed by Pearson test, Welch T-test $p<0.001$. (D) Centrin-2 centrosomal intensity based on A, n=90 cells/condition from 3 independent experiments. Average +/- SD: siControl 1 +/- 0.4 (A.U.), siWDR90: 0.68 +/- 0.4 (A.U). Mann-Whitney $p<0.001$. (E) Plot profiles of WDR90 centriolar intensity based on A, n=90 cell/condition from 3 independent experiments. (F) Plot profiles of Centrin-2 centriolar intensity based on A, n=90 cells/condition from 3 independent experiments. (G) Human U2OS cell treated with either scramble or *wdr90* and stained for POC5 (yellow) and HsSAS6 (magenta). DNA is in blue. Dotted white squares indicate insets. Scale bar: 5µm. (H) Percentage of cells with the following numbers of POC5 dots according to the number of HsSAS-6 dots per cell based on G, n=150 cells/condition from 3 independent experiments. Average +/- SD: Refer to **Table S7** (I) POC5 centrosomal intensity based on G, n=45 cells/condition from 3 independent experiments. Average +/- SD: siControl 1 +/- 0.3(A.U.), siWDR90: 0.67 +/- 0.4(A.U). Mann-Whitney $p<0.001$. (J) HsSAS-6 centrosomal intensity based on G, n=30 cells/condition from 3 independent experiments. Average +/- SD: siControl 0.99 +/- 0.3 (A.U.), siWDR90: 1 +/- 0.3 (A.U). Mann-Whitney $p=0.2551$. (K) Plot profiles of POC5 centriolar intensity based on G, n=45 cells/condition from 3 independent experiments. (L) Plot profiles of HsSAS-6 centriolar intensity based on G, n=30 cells/condition from 3 independent experiments. (M) Human U2OS cell treated with either scramble or *wdr90* siRNA and stained for CP110 (yellow) and Centrin-2 (magenta). DNA is in blue. Dotted white squares indicate insets. Scale bar: 5µm. (N) CP110 centrosomal intensity based on M, n=60 cells/condition from 3

independent experiments. Average +/- SD: siControl 1 +/- 0.4 (A.U.), siWDR90: 0.99 +/- 0.4 (A.U). Mann-Whitney p=0.7756. (O) Centrin-2 centrosomal intensity based on M, n=55 cells/condition from 3 independent experiments. Average +/- SD: siControl 1 +/- 0.3 (A.U.), siWDR90: 0.4 +/- 0.2 (A.U). Mann-Whitney $p<0.0001$. Note that Centrin-2 intensity served as an internal control for the efficient depletion of WDR90 by siRNA in this experiment.

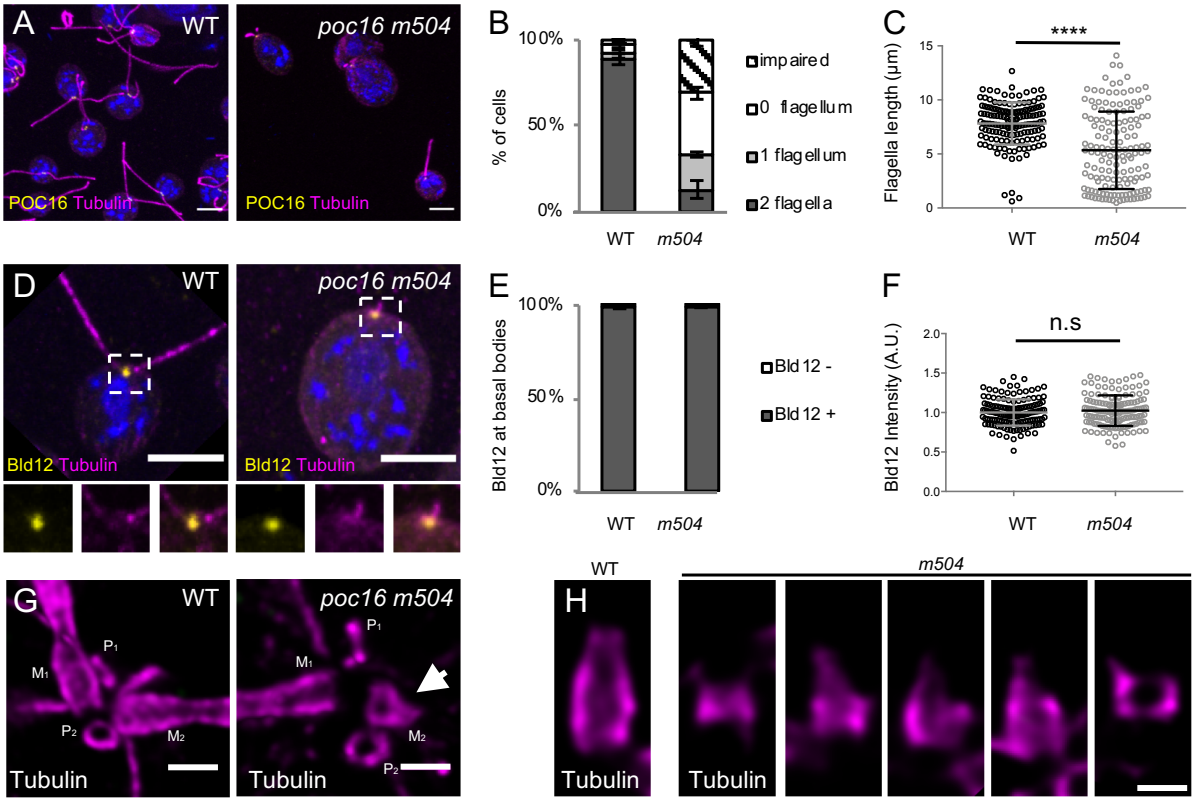

Fig. S6. POC16 is important for flagella assembly and proper centriolar structure.

(A) Confocal image of *Chlamydomonas* WT and *poc16 m504* cells stained with tubulin (magenta) and POC16 (yellow). Scale bar: 5µm (B) Percentage of cells with 0, 1, 2 or impaired flagella, n=300 cells/condition from 3 independent experiments. Average +/- SD: WT: 2 flagella= 95.5% +/- 4, 1 flagellum= 2.2% +/- 2, no flagellum= 2.3% +/- 2, impaired flagellum= 0% +/- 0; *poc16 m504:* 2 flagella= 13% +/- 5, 1 flagellum= 20% +/- 2, no flagellum: 13% +/- 3, impaired flagellum= 31% +/-3. (C) Flagellar length in µm, n=150 cells/condition from 3 independent experiments. Mann Whitney test $p<0.0001$. (D) *Chlamydomonas* WT and *poc16 m504*-mutant stained with tubulin (magenta) and Bld12 (yellow). Scale bar: 5µm (E) Percentage of cells positive for Bld12 at centrioles, n=300 cells/condition from 3 independent experiments. Average +/- SD: WT Bld12 positive (Bld12+) 99% +/- 1, *poc16m504*: 99% +/- 1. Normality

assessed by Pearson test, Welch T test p< 0.0001. (F) Bld12 fluorescence intensity, n=150 cells/condition from 3 independent experiments. Average +/- SD: WT= 1 +/- 0.01 (A.U.), *poc16m504*= 1 +/- 0.02 (A.U.). Normality assessed by Pearson test, Welch T test p=0.0714. (G) *In cellulo Chlamydomonas* WT or *poc16m504* centrioles/flagella U-ExM expanded stained for tubulin (magenta). M stands for mature centriole, P for procentriole. Arrows point to defective mature centriole. Scale bar: 400nm (H) Gallery of *poc16m504* defective short mature centrioles stained with tubulin (magenta) compared to a WT mature centriole (left panel). Scale bar: 200nm.

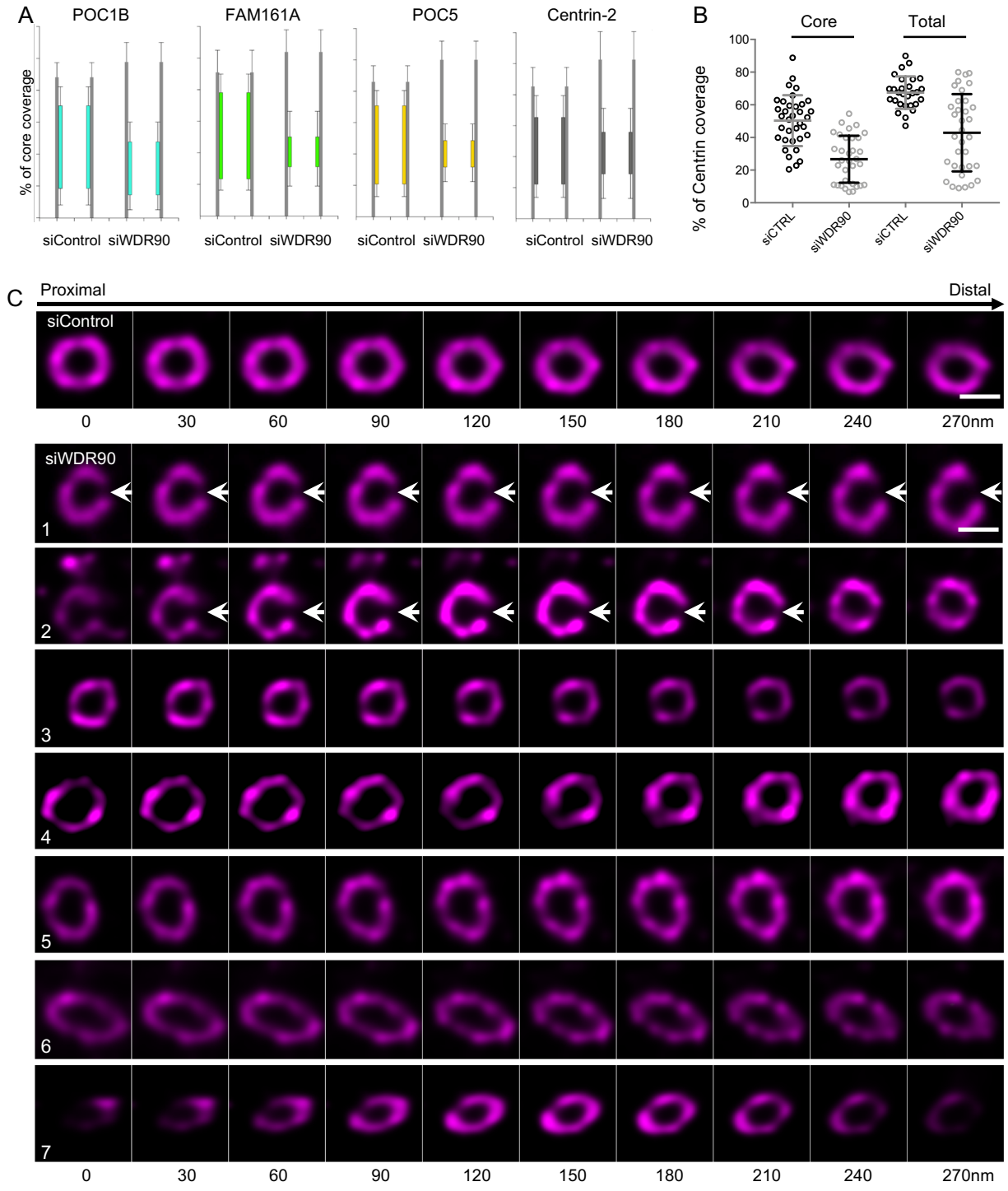

Fig. S7. WDR90 depletion leads to severe centriolar structure defects.

(A) Inner scaffold protein length and positioning based on Fig. 5D and 5E, n>30 centrioles/condition from 3 independent experiments. (B) Centrin-2 length based on Fig. 5D,

measuring inner core or total (core + distal) length. (C) *In cellulo* U-ExM expanded centriole from U2OS cells treated with siRNA targeting scramble genes or *wdr90* stained for tubulin, top views. White arrows indicate centriole fracture. Scale bar: 200nm

Table S1. Tubulin and inner scaffold proteins fluorescence intensity on microtubule triplets from external to internal.

x value for maximal intensity peak (nm)	Tubulin	Inner scaffold proteins
POC1B	53.99	68.48
FAM161A	51.36	73.75
POC5	46.09	72.43
Centrin-2	47.41	77.70

Table S2. Percentage of cells with the following number of dots/cell respectively for WDR90 and Centrin-2.

	Time		
Percentage of cells	**14hrs**	**22hrs**	**24hrs**
2--0	57 +/- 2	20 +/- 1	10 +/- 3
2--2	38 +/- 4	59 +/- 1	57 +/- 4
4--2	5 +/- 13	21 +/- 15	33 +/- 45

Table S3. Percentage of cells with the following number of dots/cell respectively for WDR90 and HsSAS-6.

	Time		
Percentage of cells	**14hrs**	**22hrs**	**24hrs**
2--0	53 +/-3	19 +/- 6	9 +/- 3
2--2	44 +/- 4	67 +/- 1	67 +/- 3
4--2	3 +/- 1	13 +/- 1	24 +/- 4

Table S4. Inner scaffold proteins length coverage.

Length coverage	siControl	siWDR90
POC1B	59 +/-14 nm	34 +/- 16 nm
FAM161A	61 +/- 9 nm	18 +/- 7 nm
POC5	56 +/- 11 nm	17 +/- 9 nm
Centrin-2	50 +/- 16 nm	27 +/- 14 nm

Table S5. Percentage of cells in each phase of the cell cycle according to post-mitotic time point.

	Time		
Percentage of cells	**14hrs**	**22hrs**	**24hrs**
G0/G1	47 +/- 10	19 +/- 10	14 +/- 5
S	43 +/- 4	39 +/- 13	17 +/- 5
G2/M	10 +/- 1	42 +/- 7	69 +/- 5

Table S6. Percentage of cells displaying 0, 1, 2 or 4 dots of WDR90 based on the number of Centrin-2 dots in U2OS cells treated with siRNA targeting scramble genes or *wdr90*.

% of cells	2 Centrin-2 dots			4 Centrin-2 dots		
	0 WDR90	1 WDR90	2 WDR90	1 WDR90	2 WDR90	4 WDR90
siControl	0 +/- 0	10 +/- 2	90 +/- 2	0 +/- 0	71 +/- 1	29 +/- 1
siWDR90	0 +/- 0	69 +/- 7	31 +/- 7	77 +/- 5	23 +/- 5	0 +/- 0

Table S7. Percentage of cells displaying 0, 1, 2 or 4 dots of POC5 based on the number of HsSas-6 dots in U2OS cells treated with siRNA targeting scramble genes or *wdr90*.

% of cells	0 HsSAS-6 dot			2 HsSas-6 dots		
	0 POC5	1 POC5	2 POC5	1 POC5	2 POC5	4 POC5
siControl	0 +/- 0	14 +/- 5	86 +/- 5	4 +/- 4	68 +/- 6	28 +/- 4
siWDR90	0 +/- 0	61 +/- 10	39 +/- 10	63 +/- 9	29 +/- 11	8 +/- 3

Captions for Movies S1 and S2.

Movie S1. Confocal stack of an U-ExM expanded WT centriole.

Top viewed *in cellulo* U-ExM expanded centriole from U2OS cell treated with scramble siRNA and stained for tubulin (magenta) and POC5 (green). Z-stack acquired every 0.12µm from the proximal to distal end of the centriole.

Movie S2. Confocal stack of an U-ExM expanded siRNA WDR90 depleted centriole.

Top viewed *in cellulo* U-ExM expanded centriole from U2OS cell treated with *wdr90* siRNA and stained for tubulin (magenta) and POC5 (green). Z-stack acquired every 0.12µm from the proximal to distal end of the centriole.

Supplementary references:

1. V. Hamel, E. Steib, R. Hamelin, F. Armand, S. Borgers, I. Flückiger, C. Busso, N. Olieric, C. O. S. Sorzano, M. O. Steinmetz, P. Guichard, P. Gönczy, Identification of Chlamydomonas Central Core Centriolar Proteins Reveals a Role for Human WDR90 in Ciliogenesis. *Curr. Biol.* **27**, 2486-2498.e6 (2017).
2. D. G. Gibson, L. Young, R.-Y. Chuang, J. C. Venter, C. A. Hutchison, H. O. Smith, Enzymatic assembly of DNA molecules up to several hundred kilobases. *Nat. Methods*. **6**, 343–345 (2009).
3. M. Schmidt-Cernohorska, I. Zhernov, E. Steib, M. Le Guennec, R. Achek, S. Borgers, D. Demurtas, L. Mouawad, Z. Lansky, V. Hamel, P. Guichard, Flagellar microtubule doublet assembly in vitro reveals a regulatory role of tubulin C-terminal tails. *Science* (2019).
4. A. Khalifa, M. Ichikawa, D. Dai, S. Kubo, C. Black, K. Peri, T. S. McAlear, S. Veyron, S. K. Yang, J. Vargas, S. Bechstedt, J.-F. Trempe, K. H. Bui, The inner junction complex of the cilia is an interaction hub that involves tubulin post-translational modifications. *bioRxiv*, 774695 (2019).